Computer Assisted Mechanics and Engineering Sciences, 7: 117–160, 2000.

Localization phenomena in thermo-viscoplastic flow processes under cyclic dynamic loadings

Wojciech Dornowski
Military University of Technology, Kaliskiego 2, 00-908 Warsaw, Poland

Piotr Perzyna
Institute of Fundamental Technological Research, Polish Academy of Sciences
Świętokrzyska 21, 00-049 Warsaw, Poland

(Received October 25, 1999)

The main objective of the paper is the investigation of localization phenomena in thermo-viscoplastic flow processes under cyclic dynamic loadings. Recent experimental observations for cycle fatigue damage mechanics at high temperature and dynamic loadings of metals suggest that the intrinsic microdamage process does very much dependent on the strain rate and the wave shape effects and is mostly developed in the regions where the plastic deformation is localized. The microdamage kinetics interacts with thermal and load changes to make failure of solids a highly rate, temperature and history dependent, nonlinear process.

A general constitutive model of elasto-viscoplastic damaged polycrystalline solids is developed within the thermodynamic framework of the rate type covariance structure with finite set of the internal state variables. A set of the internal state variables is assumed and interpreted such that the theory developed takes account of the effects as follows: (i) plastic non-normality; (ii) plastic strain induced anisotropy (kinematic hardening); (iii) softening generated by microdamage mechanisms (nucleation, growth and coalescence of microcracks); (iv) thermomechanical coupling (thermal plastic softening and thermal expansion); (v) rate sensitivity; (vi) plastic spin.

To describe suitably the time and temperature dependent effects observed experimentally and the accumulation of the plastic deformation and damage during dynamic cyclic loading process the kinetics of microdamage and the kinematic hardening law have been modified. The relaxation time is used as a regularization parameter. By assuming that the relaxation time tends to zero, the rate independent elastic-plastic response can be obtained. The viscoplastic regularization procedure assures the stable integration algorithm by using the finite difference method. Particular attention is focused on the well-posedness of the evolution problem (the initial-boundary value problem) as well as on its numerical solutions. The Lax–Richtmyer equivalence theorem is formulated and conditions under which this theory is valid are examined. Utilizing the finite difference method for regularized elasto-viscoplastic model, the numerical investigation of the three-dimensional dynamic adiabatic deformation in a particular body under cyclic loading condition is presented. Particular examples have been considered, namely dynamic, adiabatic and isothermal, cyclic loading processes for a thin steel plate with small rectangular hole located in the centre. To the upper edge of the plate the normal and parallel displacements are applied while the lower edge is supported rigidly. Both these displacements change in time cyclically. Small two asymmetric regions which undergo significant deformations and temperature rise have been determined. Their evolution until occurrence of final fracture has been simulated. The accumulation of damage and equivalent plastic deformation on each considered cycle has been obtained. It has been found that this accumulation distinctly depends on the wave shape of the assumed loading cycle.

1. Introduction

The paper aims in the investigations of localization phenomena in thermo-viscoplastic flow processes under cyclic dynamic loadings.

A number of plasticity models have been recently proposed for cyclic loadings, cf. Auricchio, Taylor and Lubliner [4], Auricchio and Taylor [5], Chaboche [6], Dafalias and Popov [16, 17], Duszek and Perzyna [24,25], Mróz [44], Ristinmaa [61], Van der Giessen [67, 68] and Wang and Ohno [70].

However none of these theories is able to describe properly the mechanism of fatigue damage when time and strain rate effects are important. Such effects have been observed by Sidey and Coffin [64]. They investigated oxygen-free high conductivity (OFHC) copper at 673 K using unequal strain rates to produce the wave shape. It has been observed that the intrinsic micro-damage process does very much depend on the strain rate effects, cf. Sec. 2.

The main objective of the present paper is the development of the thermo-elasto-viscoplasticity theory of damaged polycrystalline solids which takes into account the time and temperature dependent effects observed experimentally and the accumulation of the plastic deformation and damage during dynamic cyclic loading processes.

To describe these effects we intend to modify a constitutive model of thermo-elasto-vicsoplastic damaged polycrystalline solids developed by Duszek-Perzyna and Perzyna [26]. The main modification concerns the kinetics of microdamage and the kinematic hardening law, cf. Dornowski and Perzyna [20, 21, 22].

Next, we would like use the developed theory to the investigation of the localization of plastic deformation in complex thermo-elasto-viscoplastic flow processes under cyclic dynamic loadings.

Section 3 is devoted to the description of kinematics of finite deformations and the stress tensors. The fundamental measures of total deformation are introduced. The decomposition of the strain tensor into the elastic and viscoplastic part is presented. The rates of the deformation tensor and the stress tensor are defined based on the Lie derivative.

In Sec. 4 a general constitutive model of elasto-viscoplastic damaged polycrystalline solids is developed with the thermodynamic framework of the rate type covariance structure with a finite set of the internal state variables. A set of the internal state variables consists of the equivalent plastic deformation, volume fraction porosity and the residual stress (the back stress). The theory developed takes account of the effects as follows: (i) plastic non-normality; (ii) plastic induced anisotropy (kinematic hardening); (iii) plastic spin; (iv) softening generated by microdamage mechanisms; (v) thermomechanical coupling (thermal plastic softening and thermal expansion); (vi) rate sensitivity.

The relaxation time is used as a regularization parameter. By assuming that the relaxation time tends to zero the thermo-elastic-plastic (rate independent) response of the damaged material can be obtained.

Fracture criterion based on the evolution of microdamage is formulated.

Section 5 is devoted to the formulation of an adiabatic inelastic flow process. Basic features of a rate dependent plastic model are discussed.

In Sec. 6 the numerical solution of the initial-boundary value problem (evolution problem) is examined. Particular attention has been focused on the viscoplastic regularization procedure for the solution of the dynamical initial-boundary value problems under cyclic loadings. Convergence, consistency and stability of the discretised problem by means of the finite difference method are investigated.

The approximations based on finite difference method and the discussion of the stability condition are presented.

The Lax–Richmyer equivalence theorem is formulated and conditions under which this theorem is valid are discussed.

In Sec. 7 the identification procedure is developed and the investigation of stability and convergence of the numerical method based on finite difference approximation is presented.

Section 8 is devoted to the numerical investigation of dynamic adiabatic and isothermal, cyclic loading processes for a plate with small rectangular hole located at the centre.

In Sec. 9 the lacalization of plastic deformation and fatigue damage are investigated.

In Sec. 10 final comments are presented.

2. Experimental and physical motivations

Sidey and Coffin [64] investigated the mechanisms of fatigue as they bear on fatigue damage at elevated temperature when time and strain rate effects are important. This regime is often referred to as that of time-dependent fatigue.

Test on oxygen-free high conductivity (OFHC) copper at 673 K are examined using unequal strain rates to produce the wave shape. Some typical wave shape are shown in Fig. 1, they include equal–equal, slow–fast and fast–slow. Specimens with a gage length of 12.70 mm and diameter of 6.35 mm were used. Strain-controlled fatigue tests were carried out at 673 K in air with a total strain range of 1.0 percent. In each test the cycle time was kept constant at 600 s but the tensile and compressive strain rates were varied so that a study of wave-shape effects could be made. In the case of the unbalanced loops, the ratio of fast to slow strain rates was fixed at 100 to 1 with the slow strain rate being 1.7×10^{-5} s^{-1}. A strain rate of 3.3×10^{-5} s^{-1} was used in equal ramp rate tests. After failure, the gage-length was sectioned longitudinally for metallographic observations.

Table 1 shows the number of cycles to failure and the time to failure under the various testing conditions. It can be seen that when the total cycle time is kept constant the number of cycles to failure decreases as the tensile-going strain rate decreases.

Fig. 2 shows the failure crack in the fast–slow test. The crack path is transgranular and has started from the surface. Many transgranular surface cracks had initiated and grown for depths up to 0.5 mm but presumably these had ceased growing when one crack became dominant. No internal intergranular cracks were observed.

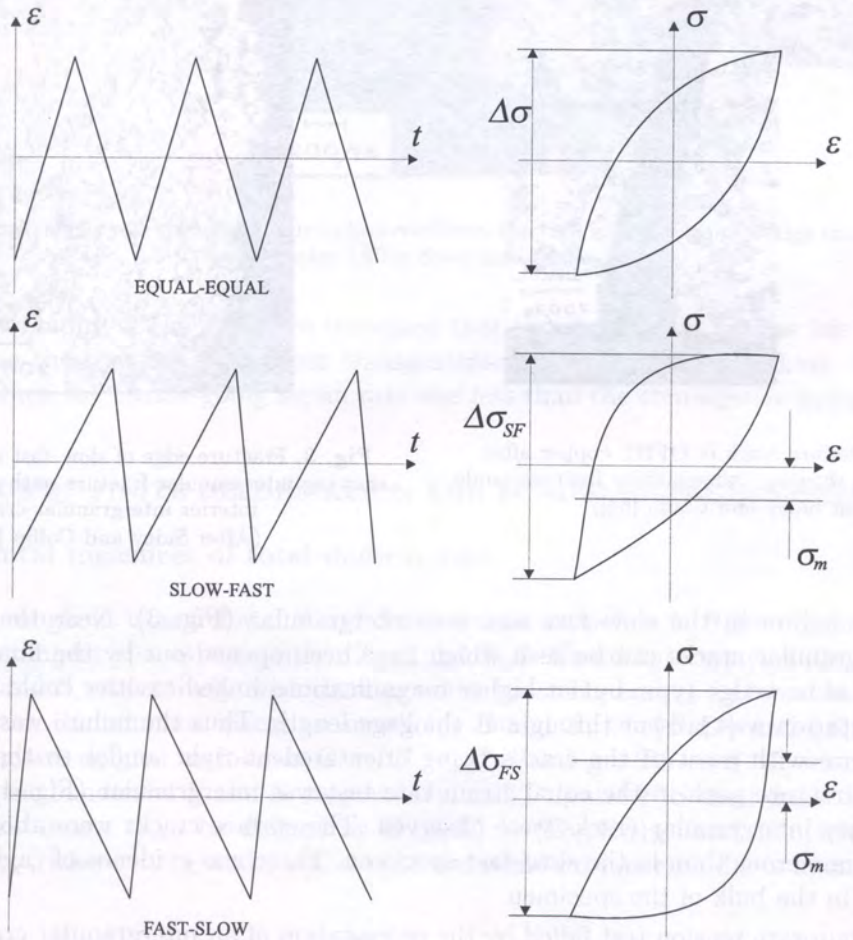

Fig. 1. Wave shapes and resulting hysteresis loops for equal and unequal forward and reserve strain rates (After Sidey and Coffin [64])

Table 1. Effect of wave-shape on the number of cycles to failure of OFHC copper at 673 K

Cycle	Slow–Fast	Equal	Fast–Slow
N_f	104	380	1138
$t_f(h)$	17	63	190

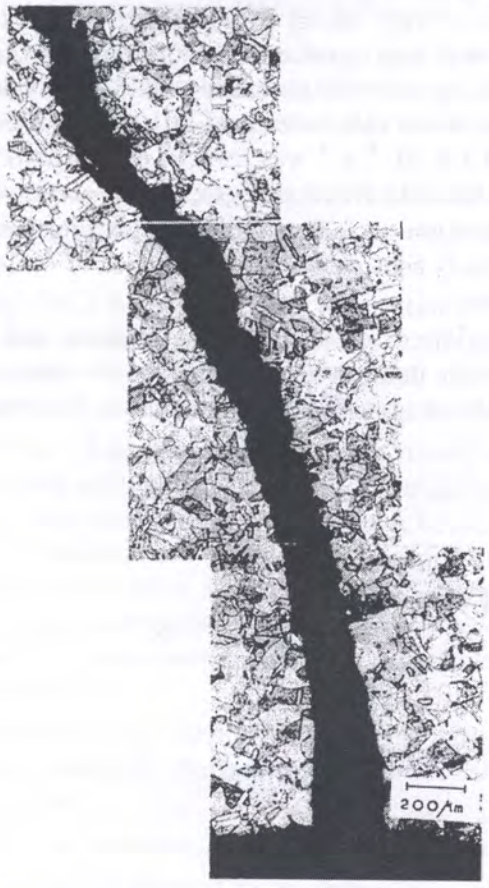

Fig. 2. Main failure crack in OFHC copper after fast–slow cycling showing transgranular fracture mode (After Sidey and Coffin [64])

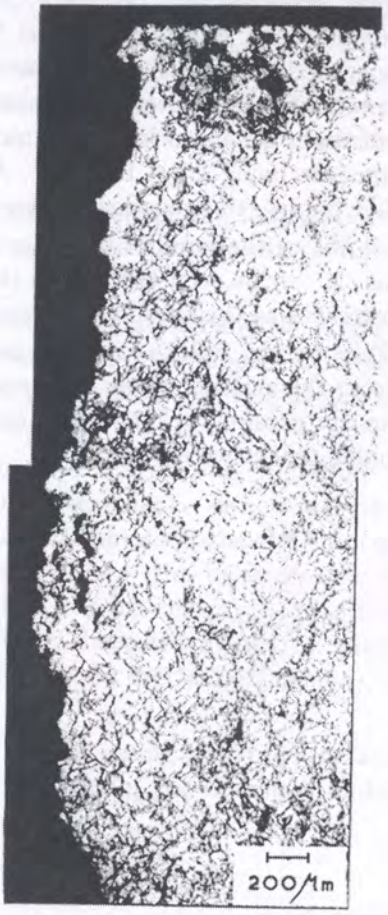

Fig. 3. Fracture edge of slow–fast cycle specimen showing intergranular fracture path and surface and interior intergranular cracks (After Sidey and Coffin [64])

In contrast, failure in the slow–fast test was intergranular (Fig. 3). Near the fracture edge, extensive intergranular cracks can be seen which have been opened out by the final failure. Many of these cracks were wedge type, but at higher magnifications linked cavities could be seen. It was noted that cavitation was present throughout the gage length. Thus the failure was typical of that for creep fracture with most of the cracks being orientated at right angles to the applied stress direction. The fracture path in the equal strain rate test was intergranular (Fig. 4). Also internal and short surface intergranular cracks were observed. The surface cracks were about one grain in depth and less numerous than in the slow–fast specimen. There was evidence of cavities either near the fracture or in the bulk of the specimen.

The slow strain rate tension test failed by the propagation of an intergranular crack. Microscopically the specimen was very similar to the equal ramp test with intergranular wedge cracks being situated near the fracture surface and no cracking in the bulk region.

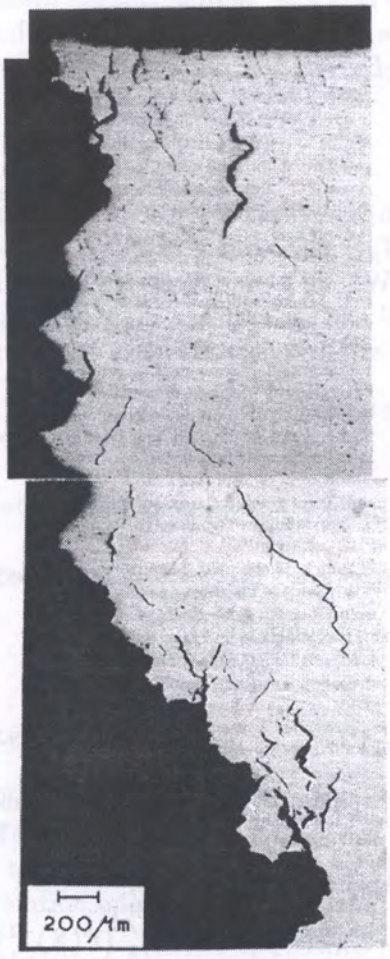

Fig. 4. Equal ramp cycle specimen in unetched condition showing interlinkage of wedge cracks near the fracture edge (After Sidey and Coffin [64])

Thus, metallography of the specimen indicated that the decrease in fatigue life was associated with a change in the fracture mode from transgranular to intergranular cracking. Cavity damage occurred only when the tensile-going strain rate was less than the compressive-going strain rate.

3. Kinematics of finite deformation and fundamental definitions

3.1. Fundamental measures of total deformation

Our notation throughout is as follows: $\mathcal{B}$ and $\mathcal{S}$ are manifolds, points in $\mathcal{B}$ are denoted $\mathbf{X}$ and those in $\mathcal{S}$ by $\mathbf{x}$. The tangent spaces are written $T_{\mathbf{X}}\mathcal{B}$ and $T_{\mathbf{x}}\mathcal{S}$. Coordinate systems are denoted $\{X^A\}$ and $\{x^a\}$ for $\mathcal{B}$ and $\mathcal{S}$, respectively, with corresponding bases $\mathbf{E}_A$ and $\mathbf{e}_a$ and dual bases $\mathbf{E}^A$ and $\mathbf{e}^a$.

Let us take the Riemannian spaces on manifolds $\mathcal{B}$ and $\mathcal{S}$, i.e. $\{\mathcal{B}, \mathbf{G}\}$ and $\{\mathcal{S}, \mathbf{g}\}$, the metric tensors $\mathbf{G}$ and $\mathbf{g}$ are defined as follows $\mathbf{G} : T\mathcal{B} \to T^*\mathcal{B}$ and $\mathbf{g} : T\mathcal{S} \to T^*\mathcal{S}$, where $T\mathcal{B}$ and $T\mathcal{S}$ denote the tangent bundles of $\mathcal{B}$ and $\mathcal{S}$, respectively, and $T^*\mathcal{B}$ and $T^*\mathcal{S}$ their dual tangent bundles.

Let the metric tensor G_{AB} be defined by $G_{AB}(\mathbf{X}) = (\mathbf{E}_A, \mathbf{E}_B)_{\mathbf{X}}$, and similarly define g_{ab} by $g_{ab}(\mathbf{x}) = (\mathbf{e}_a, \mathbf{e}_b)_{\mathbf{x}}$, where $(\ ,\ )_{\mathbf{X}}$ and $(\ ,\ )_{\mathbf{x}}$ denote the standard inner products in $\mathcal{B}$ and $\mathcal{S}$, respectively.

Let

$$\mathbf{x} = \phi(\mathbf{X}, t) \tag{1}$$

be regular motion, then $\phi_t : \mathcal{B} \to \mathcal{S}$ is a C^1 actual configuration (at time t) of $\mathcal{B}$ in $\mathcal{S}$. The tangent of ϕ is denoted $\mathbf{F}$ and is called the deformation gradient of ϕ; thus $\mathbf{F} = T\phi$. For $\mathbf{X} \in \mathcal{B}$, we let $\mathbf{F}(\mathbf{X})$ denote the restriction of $\mathbf{F}$ to $T_{\mathbf{X}}\mathcal{B}$.

Thus

$$\mathbf{F}(\mathbf{X}, t) : T_{\mathbf{X}}\mathcal{B} \to T_{\mathbf{x}=\phi(\mathbf{X},t)}\mathcal{S} \tag{2}$$

is a linear transformation for each $\mathbf{X} \in \mathcal{B}$ and $t \in I \subset \mathbb{R}$. For each $\mathbf{X} \in \mathcal{B}$ there exists an orthogonal transformation $\mathbf{R}(\mathbf{X}) : T_{\mathbf{X}}\mathcal{B} \to T_{\mathbf{x}}\mathcal{S}$ such that $\mathbf{F} = \mathbf{R} \cdot \mathbf{U} = \mathbf{V} \cdot \mathbf{R}$. Notice that $\mathbf{U}$ and $\mathbf{V}$ operate within each fixed tangent space. We call $\mathbf{U}$ and $\mathbf{V}$ the right and left stretch tensor, respectively. For each $\mathbf{X} \in \mathcal{B}$, $\mathbf{U}(\mathbf{X}) : T_{\mathbf{X}}\mathcal{B} \to T_{\mathbf{X}}\mathcal{B}$ and for each $\mathbf{x} \in \mathcal{S}$, $\mathbf{V}(\mathbf{x}) : T_{\mathbf{x}}\mathcal{S} \to T_{\mathbf{x}}\mathcal{S}$.

The material (or Lagrangian) strain tensor $\mathbf{E} : T_{\mathbf{X}}\mathcal{B} \to T_{\mathbf{X}}\mathcal{B}$ is defined by

$$2\mathbf{E} = \mathbf{C} - \mathbf{I}, \quad (\mathbf{I} \text{ denotes the identity on } T_{\mathbf{X}}\mathcal{B}), \tag{3}$$

where

$$\mathbf{C} = \mathbf{F}^T \cdot \mathbf{F} = \mathbf{U}^2 = \mathbf{B}^{-1}. \tag{4}$$

The spatial (or Eulerian) strain tensor $\mathbf{e} : T_{\mathbf{x}}\mathcal{S} \to T_{\mathbf{x}}\mathcal{S}$ is defined by

$$2\mathbf{e} = \mathbf{i} - \mathbf{c}, \quad (\mathbf{i} \text{ denotes the identity on } T_{\mathbf{x}}\mathcal{S}), \tag{5}$$

where

$$\mathbf{c} = \mathbf{b}^{-1} \quad \text{and} \quad \mathbf{b} = \mathbf{F} \cdot \mathbf{F}^T = \mathbf{V}^2. \tag{6}$$

The various strain tensors can be redefined in terms of pull-back and push-forward operations. For the material strain tensor $\mathbf{E}$ and the spatial strain tensor $\mathbf{e}$ we have

$$\begin{aligned} \mathbf{E}^\flat &= \phi^*(\mathbf{e}^\flat), & E_{AB}(\mathbf{X}) &= e_{ab}(\mathbf{x})F^a_A(\mathbf{X})F^b_B(\mathbf{X}), \\ \mathbf{e}^\flat &= \phi_*(\mathbf{E}^\flat), & e_{ab}(\mathbf{x}) &= E_{AB}(\mathbf{X})\left(\mathbf{F}(\mathbf{X})^{-1}\right)^A_a \left(\mathbf{F}(\mathbf{X})^{-1}\right)^B_b, \end{aligned} \tag{7}$$

where the symbol $\flat$ denotes the index lowering operator.

3.2. Finite elasto-viscoplastic deformation

Motivated by the micromechanics of single crystal plasticity we postulate a local multiplicative decomposition of the form

$$\mathbf{F}(\mathbf{X}, t) = \mathbf{F}^e(\mathbf{X}, t) \cdot \mathbf{F}^p(\mathbf{X}, t), \tag{8}$$

where $\mathbf{F}^{e-1}$ is interpreted as the local deformation that releases the stresses from each neighborhood $\mathcal{N}(\mathbf{x}) \subset \phi(\mathcal{B})$ in the current configuration of the body.

Let us consider a particle X, which at time $t = 0$ occupied the place $\mathbf{X}$ in the reference (material) configuration $\mathcal{B}$, its current place at time t in the actual (spatial) configuration $\mathcal{S}$ is $\mathbf{x} = \phi(\mathbf{X}, t)$ and its position in the unloaded actual configuration $\mathcal{S}'$ is denoted by $\mathbf{y}$. Thus we have

$$\mathbf{F}^e : T_{\mathbf{y}}\mathcal{S}' \to T_{\mathbf{x}}\mathcal{S}, \qquad \mathbf{F}^p : T_{\mathbf{X}}\mathcal{B} \to T_{\mathbf{y}}\mathcal{S}', \tag{9}$$

where $T_{\mathbf{y}}\mathcal{S}'$ denotes the tangent space in the unloaded actual configuration $\mathcal{S}'$. It is noteworthy that $\mathbf{F}^e$ and $\mathbf{F}^p$ defined by (9) are linear transformations.

We shall tread the tangent space $T_{\mathbf{y}}\mathcal{S}'$ as an auxiliary tool which helps to define the plastic strain tensors[1].

[1]For precise definition of the finite elasto-plastic deformation see Perzyna [55] and Duszek-Perzyna and Perzyna [27]. Different approach to define the finite elasto-plastic deformation has been presented by Nemat-Nasser [45].

The plastic strain tensor $\mathbf{E}^p : T_{\mathbf{X}}\mathcal{B} \to T_{\mathbf{X}}\mathcal{B}$ is defined by

$$\mathbf{E}^p = \frac{1}{2}(\mathbf{C}^p - \mathbf{I}), \tag{10}$$

where

$$\mathbf{C}^p = \mathbf{F}^{p^T} \cdot \mathbf{F}^p = \mathbf{U}^{p^2} = \mathbf{B}^{p^{-1}} \quad \text{and} \quad \mathbf{E}^e \overset{\text{def}}{=} \mathbf{E} - \mathbf{E}^p. \tag{11}$$

Similarly the elastic strain tensor $\mathbf{e}^e : T_x\mathcal{S} \to T_x\mathcal{S}$ is defined by

$$\mathbf{e}^e = \frac{1}{2}(\mathbf{i} - \mathbf{c}^e), \tag{12}$$

where

$$\mathbf{c}^e = \mathbf{b}^{e^{-1}}, \quad \mathbf{b}^e = \mathbf{F}^e \cdot \mathbf{F}^{e^T} = \mathbf{V}^{e^2} \quad \text{and} \quad \mathbf{e}^p \overset{\text{def}}{=} \mathbf{e} - \mathbf{e}^e. \tag{13}$$

The plastic tensors $\mathbf{E}^p$and $\mathbf{e}^p$ operate within each fixed tangent space; that is $\mathbf{E}^p : T_{\mathbf{X}}\mathcal{B} \to T_{\mathbf{X}}\mathcal{B}$ and $\mathbf{e}^p : T_{\mathbf{x}}\mathcal{S} \to T_{\mathbf{x}}\mathcal{S}$.

We can show that the following relations are valid

$$\phi_*(\mathbf{E}^{p^\flat}) = \mathbf{e}^{p^\flat}, \qquad \phi^*(\mathbf{e}^{e^\flat}) = \mathbf{E}^{e^\flat}. \tag{14}$$

3.3. Rates of the deformation tensor

Let $\phi(\mathbf{X}, t)$ be a C^2 motion of $\mathcal{B}$. Then the spatial velocity is $\boldsymbol{v}_t = \mathbf{V}_t \circ \phi_t^{-1}$, where $\mathbf{V}_t = \frac{\partial \phi}{\partial t}$ is the material velocity, i.e. $\boldsymbol{v} : \mathcal{S} \times I \to T\mathcal{S}$, $I \subset \mathbb{R}$.

The collection of maps $\phi_{t,s}$ such that for each s and $\mathbf{x}$, $t \to \phi_{t,s}(\mathbf{x})$ is an integral curve of $\boldsymbol{v}$, and $\phi_{s,s}(\mathbf{x}) = \mathbf{x}$, is called the flow or evolution operator of $\boldsymbol{v}$, i.e.

$$\{\phi_{t,s} \mid \phi_{t,s} = \phi_t \circ \phi_s^{-1} : \phi_s(\mathcal{B}) \to \phi_t(\mathcal{B})\} \tag{15}$$

and

$$\phi_{t,s} \circ \phi_{s,r} = \phi_{t,r}, \qquad \phi_{t,t} = \text{identity} \tag{16}$$

for all $r, s, t \in I \subset \mathbb{R}$.

If $\mathbf{t}$ is a C^1 (possible time-dependent) tensor field on $\mathcal{S}$, then the Lie derivative of $\mathbf{t}$ with respect to $\boldsymbol{v}$ is defined by[2]

$$\mathrm{L}_{\boldsymbol{v}}\mathbf{t} = \left(\frac{d}{dt}\phi_{t,s}^*\mathbf{t}_t\right)\Big|_{t=s}. \tag{17}$$

If we hold t fixed in $\mathbf{t}_t$, we obtain the autonomous Lie derivative

$$\mathcal{L}_{\boldsymbol{v}}\mathbf{t} = \left(\frac{d}{dt}\phi_{t,s}^*\mathbf{t}_s\right)\Big|_{t=s}. \tag{18}$$

Thus

$$\mathrm{L}_{\boldsymbol{v}}\mathbf{t} = \frac{\partial \mathbf{t}}{\partial t} + \mathcal{L}_{\boldsymbol{v}}\mathbf{t}. \tag{19}$$

If $\mathbf{t} \in \mathbf{T}^r{}_s(\mathcal{S})$ (elements of $\mathbf{T}^r{}_s(\mathcal{S})$ are called tensors on $\mathcal{S}$, contravariant of order r and covariant of order s) then $\mathrm{L}_{\boldsymbol{v}}\mathbf{t} \in \mathbf{T}^r{}_s(\mathcal{S})$.

[2]The algebraic and dynamic interpretations of the Lie derivative have been presented by Abraham et al. [1], cf. also Marsden and Hughes [43].

The spatial velocity gradient $\mathbf{l}$ is defined by

$$\mathbf{l} = D\boldsymbol{v} : T_{\mathbf{x}}\mathcal{S} \to T_{\mathbf{x}}\mathcal{S}, \qquad \text{i.e.} \quad l^a_b = v^a|_b = \frac{\partial v^a}{\partial x^b} + \gamma^a_{bc} v^c, \tag{20}$$

where γ^a_{bc} denotes the Christoffel symbol for $\mathbf{g}$.

The spatial velocity gradient $\mathbf{l}$ can be expressed as follows

$$\mathbf{l} = D\boldsymbol{v} = \dot{\mathbf{F}} \cdot \mathbf{F}^{-1} = \dot{\mathbf{F}}^e \cdot \mathbf{F}^{e^{-1}} + \mathbf{F}^e \cdot \left(\dot{\mathbf{F}}^p \cdot \mathbf{F}^{p^{-1}}\right) \cdot \mathbf{F}^{e^{-1}} = \mathbf{l}^e + \mathbf{l}^p = \mathbf{d} + \boldsymbol{\omega} = \mathbf{d}^e + \boldsymbol{\omega}^e + \mathbf{d}^p + \boldsymbol{\omega}^p, \tag{21}$$

where $\mathbf{d}$ denotes the spatial rate of deformation tensor and $\boldsymbol{\omega}$ is called the spin.

Let us define the material (or Lagrangian) rate of deformation tensor $\mathbf{D}$ as follows

$$\mathbf{D}(\mathbf{X}, t) = \frac{\partial}{\partial t}\mathbf{E}(\mathbf{X}, t). \tag{22}$$

We have very important relation

$$\mathbf{d}^\flat = \mathrm{L}_{\boldsymbol{v}}\mathbf{e}^\flat = \phi_* \frac{\partial}{\partial t}\left(\phi^* \mathbf{e}^\flat\right) = \phi_*\left(\frac{\partial}{\partial t}\mathbf{E}^\flat\right) = \phi_*\left(\mathbf{D}^\flat\right). \tag{23}$$

On the other hand

$$\mathbf{d}^\flat = \mathrm{L}_{\boldsymbol{v}}\mathbf{e}^\flat = \mathrm{L}_{\boldsymbol{v}}\left[\frac{1}{2}\left(\mathbf{g} - \mathbf{b}^{-1}\right)\right]^\flat = \frac{1}{2}\mathrm{L}_{\boldsymbol{v}}\mathbf{g} = \frac{1}{2}\left(g_{cb} v^c|_a + g_{ac} v^c|_b\right) \mathbf{e}^a \otimes \mathbf{e}^b, \tag{24}$$

i.e. the symmetric part of the velocity gradient $\mathbf{l}$ (the symbol $\otimes$ denotes the tensor product).

The components of the spin $\boldsymbol{\omega}$ are given by

$$\omega_{ab} = \frac{1}{2}\left(g_{ac} v^c|_b - g_{cb} v^c|_a\right) = \frac{1}{2}\left(\frac{\partial v_a}{\partial x^b} - \frac{\partial v_b}{\partial x^a}\right), \tag{25}$$

and

$$\mathbf{d}^{e^\flat} = \mathrm{L}_{\boldsymbol{v}}\mathbf{e}^{e^\flat}, \qquad \mathbf{d}^{p^\flat} = \mathrm{L}_{\boldsymbol{v}}\mathbf{e}^{p^\flat}. \tag{26}$$

3.4. Rates of the stress tensors

The first Piola–Kirchhoff stress tensor P^{aA} is the two-point tensor obtained by performing a Piola transformation on the second index of the Cauchy stress tensor $\boldsymbol{\sigma}$, i.e.

$$P^{aA} = J(\mathbf{F}^{-1})^A_b \, \sigma^{ab}, \tag{27}$$

where J denotes the Jacobian of the deformation.

The second Piola–Kirchhoff stress tensor $\mathbf{S}$ is defined as follows

$$S^{AB} = (\mathbf{F}^{-1})^A_a \, P^{aB} = J(\mathbf{F}^{-1})^A_a \, (\mathbf{F}^{-1})^B_b \, \sigma^{ab} = (\mathbf{F}^{-1})^A_a \, (\mathbf{F}^{-1})^B_b \, \tau^{ab}, \tag{28}$$

i.e.

$$\mathbf{S} = \phi^*(\boldsymbol{\tau}), \tag{29}$$

where $\boldsymbol{\tau} = J\boldsymbol{\sigma}$ is called the Kirchhoff stress tensor.

The rate of the Kirchhoff stress tensor $\boldsymbol{\tau}$ is given by

$$\mathrm{L}_{\boldsymbol{v}}\boldsymbol{\tau} = \phi_* \frac{\partial}{\partial t}(\phi^* \boldsymbol{\tau}) = \phi_*\left(\frac{\partial}{\partial t}\mathbf{S}\right) = \mathbf{F} \cdot \left(\frac{\partial}{\partial t}\mathbf{S}\right) \cdot \mathbf{F}^T \circ \phi_t^{-1}. \tag{30}$$

Let us define

$$\boldsymbol{\tau}_1 = \tau^{ab}\,\mathbf{e}_a \otimes \mathbf{e}_b \in \mathbf{T}^2{}_0(\mathcal{S}), \qquad \boldsymbol{\tau}_2 = \tau_a{}^b\,\mathbf{e}^a \otimes \mathbf{e}_b \in \mathbf{T}_1{}^1(\mathcal{S}), \qquad \boldsymbol{\tau}_3 = \tau^a{}_b\,\mathbf{e}_a \otimes \mathbf{e}^b \in \mathbf{T}^1{}_1(\mathcal{S}). \tag{31}$$

Then

$$(\mathrm{L}_{\boldsymbol{v}}\boldsymbol{\tau}_1)^{ab} = \frac{\partial \tau^{ab}}{\partial t} + \frac{\partial \tau^{ab}}{\partial x^c}\,v^c - \tau^{cb}\,\frac{\partial v^a}{\partial x^c} - \tau^{ac}\,\frac{\partial v^b}{\partial x^c}\,. \tag{32}$$

is the rate associated with the name Oldroyd (cf. Oldroyd [47]). The Zaremba–Jaumann rate (cf. Zaremba [71, 72] and Jaumann [32]) is defined as follows

$$\frac{1}{2}\left[(\mathrm{L}_{\boldsymbol{v}}\boldsymbol{\tau}_3)^a{}_c\,g^{cb} + g^{ac}\,(\mathrm{L}_{\boldsymbol{v}}\boldsymbol{\tau}_2)_c{}^b\right] = \frac{\partial \tau^{ab}}{\partial t} + \frac{\partial \tau^{ab}}{\partial x^c}\,v^c + \tau^{ad}\,\omega_d{}^b - \tau^{db}\,\omega^a{}_d\,. \tag{33}$$

4. Constitutive modelling for dynamic cyclic loadings

4.1. Constitutive postulates and fundamental assumptions

Let us assume that: (i) conservation of mass, (ii) balance of momentum, (iii) balance of moment of momentum, (iv) balance of energy, (v) entropy production inequality hold.

We introduce the four fundamental postulates:

(i) Existence of the free energy function. It is assumed that the free energy function is given by

$$\psi = \hat{\psi}(\mathbf{e}, \mathbf{F}, \vartheta; \boldsymbol{\mu}), \tag{34}$$

where $\mathbf{e}$ denotes the Eulerian strain tensor, $\mathbf{F}$ is deformation gradient, ϑ temperature and $\boldsymbol{\mu}$ denotes a set of the internal state variables.

To extend the domain of the description of the material properties and particularly to take into consideration diferent dissipation effects we have to introduce the internal state variables represented by the vector $\boldsymbol{\mu}$.

(ii) Axiom of objectivity (spatial covariance). The constitutive structure should be invariant with respect to any diffeomorphism (any motion) $\boldsymbol{\xi} : \mathcal{S} \to \mathcal{S}$ (Marsden and Hughes [43]). Assuming that $\boldsymbol{\xi} : \mathcal{S} \to \mathcal{S}$ is a regular, orientation preserving map transforming $\mathbf{x}$ into $\mathbf{x}'$ and $T\boldsymbol{\xi}$ is an isometry from $T_{\mathbf{x}}\mathcal{S}$ to $T_{\mathbf{x}'}\mathcal{S}$, we obtain the axiom of material frame indifference (cf. Truesdell and Noll [66]).

(iii) The axiom of the entropy production. For any regular motion of single crystal (denoted by $\mathcal{B}$) the constitutive functions are assumed to satisfy the reduced dissipation inequality

$$\frac{1}{\rho_{Ref}}\,\boldsymbol{\tau} : \mathbf{d} - (\eta\dot{\vartheta} + \dot{\psi}) - \frac{1}{\rho\vartheta}\,\mathbf{q}\cdot\mathrm{grad}\vartheta \geq 0, \tag{35}$$

where ρ_{Ref} and ρ denote the mass density in the reference and actual configuration, respectively, $\boldsymbol{\tau}$ is the Kirchhoff stress tensor, $\mathbf{d}$ the rate defomation, η is the specific (per unit mass) entropy, and $\mathbf{q}$ denotes the heat flow vector field. Marsden and Hughes [43] proved that the reduced dissipation inequality (35) is equivalent to the entropy production inequality first introduced by Coleman and Noll [8] in the form of the Clausius–Duhem inequality. In fact the Clausius–Duhem inequality gives a statement of the second law of thermodynamics within the framework of mechanics of continuous media.

(iv) The evolution equation for the internal state variable vector $\boldsymbol{\mu}$ is assumed in the form as follows

$$\mathrm{L}_{v}\boldsymbol{\mu} = \hat{\mathbf{m}}(\mathbf{e}, \mathbf{F}, \vartheta, \boldsymbol{\mu}), \tag{36}$$

where the evolution function $\hat{\mathbf{m}}$ has to be determined based on careful physical interpretation of a set of the internal state variables and analysis of available experimental observations.

The determination of the evolution function $\hat{\mathbf{m}}$ (in practice a finite set of the evolution functions) appears to be the main problem of the modern constitutive modelling.

The main objective is to develop the rate type constitutive structure for an elastic-viscoplastic material in which the effects of the plastic non-normality, plastic spin, plastic strain induced anisotropy (kinematic hardening), micro-damaged mechanism and thermomechanical coupling are taken into consideration. To do this it is sufficient to assume a finite set of the internal state variables. Let us postulate

$$\boldsymbol{\mu} = (\boldsymbol{\zeta}, \xi, \boldsymbol{\alpha}), \tag{37}$$

where $\boldsymbol{\zeta}$ denotes the new internal state vector which describes the dissipation effects generated by viscoplastic flow phenomena, ξ is volume fraction porosity and takes account for micro-damaged effects and $\boldsymbol{\alpha}$ denotes the residual stress (the back stress) and aims at the description of the kinematic hardening effects.

Let us introduce the plastic potential function $f = f(\tilde{J}_1, \tilde{J}_2, \vartheta, \boldsymbol{\mu})$, where $\tilde{J}_1$, $\tilde{J}_2$ denote the first two invariants of the stress tensor $\tilde{\boldsymbol{\tau}} = \boldsymbol{\tau} - \boldsymbol{\alpha}$.

Let us postulate the evolution equations as follows

$$\mathbf{d}^p = \Lambda \mathbf{P}, \qquad \boldsymbol{\omega}^p = \Lambda \boldsymbol{\Omega}, \qquad \mathrm{L}_{v}\boldsymbol{\zeta} = \Lambda \mathbf{Z}, \qquad \dot{\xi} = \Xi, \qquad \mathrm{L}_{v}\boldsymbol{\alpha} = \mathbf{A}, \tag{38}$$

where for elasto-viscoplastic model of a material we assume (cf. Perzyna [48, 49, 50, 55])

$$\Lambda = \frac{1}{T_m} \left\langle \Phi\left(\frac{f}{\kappa} - 1\right) \right\rangle, \tag{39}$$

T_m denotes the relaxation time for mechanical disturbances, the isotropic work-hardening-softening function κ is

$$\kappa = \hat{\kappa}(\epsilon^p, \vartheta, \xi), \qquad \epsilon^p = \int_0^t \left(\frac{2}{3}\mathbf{d}^p : \mathbf{d}^p\right)^{\frac{1}{2}} \mathrm{d}t, \tag{40}$$

Φ is the empirical overstress function, the bracket $\langle \cdot \rangle$ defines the ramp function,

$$\mathbf{P} = \left.\frac{\partial f}{\partial \boldsymbol{\tau}}\right|_{\xi=const} \left(\left\| \frac{\partial f}{\partial \boldsymbol{\tau}} \right\|\right)^{-1}, \tag{41}$$

$\boldsymbol{\Omega}$, $\mathbf{Z}$, Ξ and $\mathbf{A}$ denote the evolution functions which have to be determined.

It is noteworthy that the material function $\mathbf{Z}$ is intrinsically determined by the constitutive assumptions postulated. To show this it is sufficient to perform a Legendre transformation as has been presented by Duszek and Perzyna [25].

For our practical purposes it is sufficient to assume that the internal state vector $\boldsymbol{\zeta}$ is equal to the equivalent plastic deformation ϵ^p, i.e.

$$\boldsymbol{\mu} = (\epsilon^p, \xi, \boldsymbol{\alpha}). \tag{42}$$

Then the material function Z is directly determined from

$$\dot{\epsilon}^p = \Lambda Z = \left(\frac{2}{3}\mathbf{d}^p : \mathbf{d}^p\right)^{\frac{1}{2}} = \sqrt{\frac{2}{3}}\Lambda, \tag{43}$$

i.e.

$$Z = \sqrt{\frac{2}{3}}. \tag{44}$$

4.2. Constitutive assumption for the plastic spin

The constitutive laws for the plastic spin[3] based on the application of the tensor function formulation have been proposed by Mandel [40, 41], Kratochvil [35], Dafalias [11, 13, 14, 15] and Loret [36, 37]. Different proposition by using generalized normality condition has been introduced by Halphen [29], Mandel [42], Dafalias [12] and Van der Giessen [67,68].

Let us postulate that $\boldsymbol{\Omega}$ has the form (cf. Dafalias [11] and Loret [36])

$$\boldsymbol{\Omega} = \eta^*(\boldsymbol{\alpha} \cdot \mathbf{P} - \mathbf{P} \cdot \boldsymbol{\alpha}), \tag{45}$$

where η^* denotes the scalar valued function of the invariants of the tensors $\boldsymbol{\alpha}$ and $\mathbf{P}$, and may depend on temperature ϑ and porosity ξ.

4.3. Intrinsic micro-damage process

An analysis of the experimental observations for cycle fatigue damage mechanisms at high temperature of metals performed by Sidey and Coffin [64] suggests that the intrinsic micro-damage process does very much depend on the strain rate effects as well as on the wave shape effects. In the tests in which duration of extension stress was larger than duration of compression stress (in single cycle) decreasing of the fatigue lifetime was observed and fracture mode changed from a transgranular fracture for the fast–slow wave shape to an intergranular single-crack fracture for equal ramp rates to interior cavitation for the slow–fast test.

To take into consideration these observed time dependent effects it is advantageous to use the proposition of the description of the intrinsic micro-damage process presented by Perzyna [52, 53] and Duszek-Perzyna and Perzyna [26].

Let us assume that the intrinsic micro-damage process consists of the nucleation and growth mechanism[4].

Physical considerations (cf. Curran et al. [10] and Perzyna [52, 53]) have shown that the nucleation of microvoids in dynamic loading processes which are characterized by very short time duration is governed by the thermally-activated mechanism. Based on this heuristic suggestion and taking into account the influence of the stress triaxiality on the nucleation mechanism we postulate for rate dependent plastic flow

$$\left(\dot{\xi}\right)_{nucl} = \frac{1}{T_m} h^*(\xi, \vartheta) \left[\exp \frac{m^*(\vartheta)\, |\tilde{I}_n - \tau_n(\xi, \vartheta, \epsilon^p)|}{k\vartheta} - 1 \right], \tag{46}$$

where k denotes the Boltzmann constant, $h^*(\xi, \vartheta)$ represents a void nucleation material function which is introduced to take account of the effect of microvoid interaction, $m^*(\vartheta)$ is a temperature dependent coefficient, $\tau_n(\xi, \vartheta, \epsilon^p)$ is the porosity, temperature and equivalent plastic strain dependent threshold stress for microvoid nucleation,

$$\tilde{I}_n = a_1 \tilde{J}_1 + a_2 \sqrt{\tilde{J}_2'} + a_3 \left(\tilde{J}_3'\right)^{\frac{1}{3}} \tag{47}$$

defines the stress intensity invariant for nucleation, a_i $(i = 1, 2, 3)$ are the material constants, $\tilde{J}_1$ denotes the first invariant of the stress tensor $\tilde{\boldsymbol{\tau}} = \boldsymbol{\tau} - \boldsymbol{\alpha}$, $\tilde{J}_2'$ and $\tilde{J}_3'$ are the second and third invariants of the stress deviator $\tilde{\boldsymbol{\tau}}' = (\boldsymbol{\tau} - \boldsymbol{\alpha})'$.

[3] For a thorough discussion of a concept of the plastic spin and its constitutive description in phenomenological theories for macroscopic large plastic deformations please consult the critical review paper by Van der Giessen [69].

[4] Recent experimental observation results (cf. Shockey et al. [63]) have shown that coalescence mechanism can be treated as nucleation and growth process on a smaller scale. This conjecture simplifies very much the description of the intrinsic micro-damage process by taking account only of the nucleation and growth mechanisms.

For the growth mechanism we postulate (cf. Johnson [33]; Perzyna [52, 53]; Perzyna and Drabik [56, 57])

$$\left(\dot{\xi}\right)_{grow} = \frac{1}{T_m} \frac{g^*(\xi,\vartheta)}{\sqrt{\kappa_0}} \left[\tilde{I}_g - \tau_{eq}(\xi,\vartheta,\epsilon^p)\right], \tag{48}$$

where $T_m\sqrt{\kappa_0}$ denotes the dynamic viscosity of a material, $g^*(\xi,\vartheta)$ represents a void growth material function and takes account for void interaction, $\tau_{eq}(\xi,\vartheta,\epsilon^p)$ is the porosity, temperature and equivalent plastic strain dependent void growth threshold stress,

$$\tilde{I}_g = b_1\tilde{J}_1 + b_2\sqrt{\tilde{J}_2'} + b_3\left(\tilde{J}_3'\right)^{\frac{1}{3}}, \tag{49}$$

defines the stress intensity invariant for growth and b_i $(i = 1,2,3)$ are the material constants.

Finally the evolution equation for the porosity ξ has the form

$$\dot{\xi} = \frac{h^*(\xi,\vartheta)}{T_m}\left[\exp\frac{m^*(\vartheta)\,|\tilde{I}_n - \tau_n(\xi,\vartheta,\epsilon^p)|}{k\vartheta} - 1\right] + \frac{g^*(\xi,\vartheta)}{T_m\sqrt{\kappa_0}}\left[\tilde{I}_g - \tau_{eq}(\xi,\vartheta,\epsilon^p)\right]. \tag{50}$$

This determines the evolution function Ξ.

4.4. Kinematic hardening

For a constitutive model describing the behaviour of a material under cyclic loading processes the crucial role plays the evolution equation for the back stress $\boldsymbol{\alpha}$, which is responsible for the description of the induced plastic strain anisotropy effects.

We shall follow some fundamental results obtained by Duszek and Perzyna [24]. Let us postulate

$$\mathrm{L}_v\boldsymbol{\alpha} = A(\mathbf{d}^p, \tilde{\boldsymbol{\tau}}, \vartheta, \xi). \tag{51}$$

Making use of the tensorial representation of the function A and taking into account that there is no change of $\boldsymbol{\alpha}$ when $\tilde{\boldsymbol{\tau}} = 0$ and $\mathbf{d}^p = 0$ the evolution law (51) can be written in the form (cf. Truesdell and Noll [66])

$$\begin{aligned}\mathrm{L}_v\boldsymbol{\alpha} = {} & \eta_1\mathbf{d}^p + \eta_2\tilde{\boldsymbol{\tau}} + \eta_3\mathbf{d}^{p^2} + \eta_4\tilde{\boldsymbol{\tau}}^2 + \eta_5\left(\mathbf{d}^p\cdot\tilde{\boldsymbol{\tau}} + \tilde{\boldsymbol{\tau}}\cdot\mathbf{d}^p\right) \\ & + \eta_6\left(\mathbf{d}^{p^2}\cdot\tilde{\boldsymbol{\tau}} + \tilde{\boldsymbol{\tau}}\cdot\mathbf{d}^{p^2}\right) + \eta_7\left(\mathbf{d}^p\cdot\tilde{\boldsymbol{\tau}}^2 + \tilde{\boldsymbol{\tau}}^2\cdot\mathbf{d}^p\right) + \eta_8\left(\mathbf{d}^{p^2}\cdot\tilde{\boldsymbol{\tau}}^2 + \tilde{\boldsymbol{\tau}}^2\cdot\mathbf{d}^{p^2}\right),\end{aligned} \tag{52}$$

where $\eta_1,\ldots,\eta_8$ are functions of the basic invariant of $\mathbf{d}^p$ and $\tilde{\boldsymbol{\tau}}$, the porosity parameter ξ and temperature ϑ.

A linear approximation of the general evolution law (52) leads to the result

$$\mathrm{L}_v\boldsymbol{\alpha} = \eta_1\mathbf{d}^p + \eta_2\tilde{\boldsymbol{\tau}}. \tag{53}$$

This kinetic law (53) represents the linear combination of the Prager and Ziegler kinematic hardening rules (cf. Prager [58] and Ziegler [73]).

To determine the connection between the material functions η_1 and η_2 we take advantage of the geometrical relation (cf. Duszek and Perzyna [24, 25])

$$(\mathrm{L}_v\boldsymbol{\alpha} - r\mathbf{d}^p) : \mathbf{Q} = 0, \tag{54}$$

where

$$\mathbf{Q} = \left[\frac{\partial f}{\partial\boldsymbol{\tau}} + \left(\frac{\partial f}{\partial\xi} - \frac{\partial\kappa}{\partial\xi}\right)\frac{\partial\xi}{\partial\boldsymbol{\tau}}\right]\left\|\frac{\partial f}{\partial\boldsymbol{\tau}} + \left(\frac{\partial f}{\partial\xi} - \frac{\partial\kappa}{\partial\xi}\right)\frac{\partial\xi}{\partial\boldsymbol{\tau}}\right\|^{-1}, \tag{55}$$

and r denotes the new material function.

The relation (54) leads to the result

$$\eta_2 = \frac{1}{T_m}\left\langle \Phi\left(\frac{f}{\kappa}-1\right)\right\rangle [r(\xi,\vartheta)-\eta_1]\,\frac{\mathbf{P}:\mathbf{Q}}{\tilde{\boldsymbol{\tau}}:\mathbf{Q}}\,. \tag{56}$$

Finally the kinematic hardening evolution law takes the form

$$\mathrm{L}_{\upsilon}\boldsymbol{\alpha} = \frac{1}{T_m}\left\langle \Phi\left(\frac{f}{\kappa}-1\right)\right\rangle \left[r_1(\xi,\vartheta)\mathbf{P} + r_2(\xi,\vartheta)\,\frac{\mathbf{P}:\mathbf{Q}}{\tilde{\boldsymbol{\tau}}:\mathbf{Q}}\tilde{\boldsymbol{\tau}}\right], \tag{57}$$

where

$$r_1(\xi,\vartheta) = \eta_1, \qquad r_2(\xi,\vartheta) = r-\eta_1\,. \tag{58}$$

It is noteworthy to add that the developed procedure can be used as general approach for obtaining various particular kinematic hardening laws. As an example let us assume that the evolution function A in (51) instead of $\mathbf{d}^p$ and $\tilde{\boldsymbol{\tau}}$ depends on $\mathbf{d}^p$ and $\boldsymbol{\alpha}$ only (cf. Agah-Tehrani et al. [2]). Then instead of (57) we obtain

$$\mathrm{L}_{\upsilon}\boldsymbol{\alpha} = \frac{1}{T_m}\left\langle \Phi\left(\frac{f}{\kappa}-1\right)\right\rangle [\zeta_1(\xi,\vartheta)\mathbf{P} - \zeta_2(\xi,\vartheta)\boldsymbol{\alpha}], \tag{59}$$

where

$$\zeta_1 = r_1, \qquad \zeta_2 = -r_2(\xi,\vartheta)\,\frac{\mathbf{P}:\mathbf{Q}}{\boldsymbol{\alpha}:\mathbf{Q}}\,. \tag{60}$$

When the infinitesimal deformations and rate independent response of a material are assumed and the intrinsic micro-damage effects are neglected then the kinematic hardening law (59) reduces to that proposed by Armstrong and Frederick [3].

The kinematic hardening law (59) leads to the nonlinear stress–strain relation with the characteristic saturation effect. The material function $\zeta_1(\xi,\vartheta)$ for $\xi=\xi_0$ and $\vartheta=\vartheta_0$ can be interpreted as an initial value of the kinematic hardening modulus while the material function $\zeta_2(\xi,\vartheta)$ determines the character of the nonlinearity of kinematic hardening. The particular forms of the functions ζ_1 and ζ_2 have to take into account the degradation nature of the influence of the intrinsic micro-damage process on the evolution of anisotropic hardening.

4.5. Thermodynamic restrictions and rate type constitutive relations

Suppose the axiom of the entropy production holds. Then the constitutive assumption (34) and the evolution equations (38) lead to the results as follows

$$\boldsymbol{\tau} = \rho_{Ref}\frac{\partial\hat{\psi}}{\partial\mathbf{e}}\,, \qquad \eta = -\frac{\partial\hat{\psi}}{\partial\vartheta}\,, \qquad -\frac{\partial\hat{\psi}}{\partial\boldsymbol{\mu}}\cdot\mathrm{L}_{\upsilon}\boldsymbol{\mu} - \frac{1}{\rho\vartheta}\mathbf{q}\cdot\mathrm{grad}\vartheta \geq 0. \tag{61}$$

The rate of internal dissipation is determined by

$$\vartheta\hat{i} = -\frac{\partial\hat{\psi}}{\partial\boldsymbol{\mu}}\cdot\mathrm{L}_{\upsilon}\boldsymbol{\mu} = -\left[\frac{\partial\hat{\psi}}{\partial\epsilon^p}\sqrt{\frac{2}{3}} + \frac{\partial\hat{\psi}}{\partial\boldsymbol{\alpha}}:\left(r_1\mathbf{P} + r_2\,\frac{\mathbf{P}:\mathbf{Q}}{\tilde{\boldsymbol{\tau}}:\mathbf{Q}}\,\tilde{\boldsymbol{\tau}}\right)\right]\Lambda - \frac{\partial\hat{\psi}}{\partial\xi}\,\Xi. \tag{62}$$

Operating on the stress relation $(61)_1$ with the Lie derivative and keeping the internal state vector constant, we obtain (cf. Duszek–Perzyna and Perzyna [25, 26])

$$\mathrm{L}_{\upsilon}\boldsymbol{\tau} = \mathcal{L}^e:\mathbf{d} - \mathcal{L}^{th}\dot{\vartheta} - [(\mathcal{L}^e+\mathbf{g}\boldsymbol{\tau}+\boldsymbol{\tau}\mathbf{g}+\mathcal{W}):\mathbf{P}]\,\frac{1}{T_m}\left\langle \Phi\left(\frac{f}{\kappa}-1\right)\right\rangle, \tag{63}$$

where

$$\mathcal{L}^e = \rho_{Ref} \frac{\partial^2 \hat{\psi}}{\partial \mathbf{e}^2}, \qquad \mathcal{L}^{th} = -\rho_{Ref} \frac{\partial^2 \hat{\psi}}{\partial \mathbf{e} \partial \vartheta}, \qquad \mathcal{W} = \eta^*[(\mathbf{g}\boldsymbol{\tau} - \boldsymbol{\tau}\mathbf{g}) : (\boldsymbol{\alpha}\mathbf{g} - \mathbf{g}\boldsymbol{\alpha})]. \tag{64}$$

Substituting $\dot{\psi}$ into the energy balance equation and taking into account the results $(61)_3$ and (62) gives

$$\rho \vartheta \dot{\eta} = -\operatorname{div} \mathbf{q} + \rho \vartheta \hat{i}. \tag{65}$$

Operating on the entropy relation $(61)_2$ with the Lie derivative and substituting the result into (65) we obtain

$$\rho c_p \dot{\vartheta} = -\operatorname{div} \mathbf{q} + \vartheta \frac{\rho}{\rho_{Ref}} \frac{\partial \boldsymbol{\tau}}{\partial \vartheta} : \mathbf{d} + \rho \chi^* \boldsymbol{\tau} : \mathbf{d}^p + \rho \chi^{**} \dot{\xi}, \tag{66}$$

where the specific heat

$$c_p = -\vartheta \frac{\partial^2 \hat{\psi}}{\partial \vartheta^2} \tag{67}$$

and the irreversibility coefficients χ^* and χ^{**} are determined by

$$\begin{aligned} \chi^* &= -\left[\left(\frac{\partial \hat{\psi}}{\partial \epsilon^p} - \vartheta \frac{\partial^2 \hat{\psi}}{\partial \vartheta \partial \epsilon^p} \right) \sqrt{\frac{2}{3}} + \left(\frac{\partial \hat{\psi}}{\partial \boldsymbol{\alpha}} - \vartheta \frac{\partial^2 \hat{\psi}}{\partial \vartheta \partial \boldsymbol{\alpha}} \right) : \left(r_1 \mathbf{P} + r_2 \frac{\mathbf{P} : \mathbf{Q}}{\tilde{\boldsymbol{\tau}} : \mathbf{Q}} \tilde{\boldsymbol{\tau}} \right) \right] \frac{1}{\boldsymbol{\tau} : \mathbf{P}}, \\ \chi^{**} &= -\left(\frac{\partial \hat{\psi}}{\partial \xi} - \vartheta \frac{\partial^2 \hat{\psi}}{\partial \vartheta \partial \xi} \right). \end{aligned} \tag{68}$$

4.6. Fracture criterion based on the evolution of microdamage

We base the fracture criterion on the evolution of the porosity internal state variable ξ. The volume fraction porosity ξ takes account for microdamage effects.

Let us assume that for $\xi = \xi^F$ catastrophe takes place (cf. Perzyna [51]), that is

$$\kappa = \hat{\kappa}(\epsilon^p, \vartheta, \xi)|_{\xi = \xi^F} = 0. \tag{69}$$

It means that for $\xi = \xi^F$ the material loses its carrying capacity. The condition (69) describes the main feature observed experimentally that the load tends to zero at the fracture point.

In is noteworthy that the isotropic hardening-softening material function $\hat{\kappa}$ proposed in Eq. $(40)_1$ should satisfy the fracture criterion (69).

5. Adiabatic inelastic flow process

5.1. Formulation of an adiabatic inelastic flow process

Let us define an adiabatic inelastic flow process as follows (cf. Perzyna [54, 55]). Find ϕ, $\boldsymbol{v}$, ρ, $\boldsymbol{\tau}$, $\boldsymbol{\alpha}$, ξ and ϑ as function of t and $\mathbf{x}$ such that

(i) the field equations

$$
\begin{aligned}
\dot{\phi} &= \boldsymbol{v}, \\
\dot{\boldsymbol{v}} &= \frac{1}{\rho_{Ref}} \left(\frac{\boldsymbol{\tau}}{\rho} \operatorname{grad} \rho + \operatorname{div} \boldsymbol{\tau} \right), \\
\dot{\rho} &= -\rho \operatorname{div} \boldsymbol{v}, \\
\dot{\boldsymbol{\tau}} &= \left(\mathcal{L}^e - \frac{\vartheta}{c_p \rho_{Ref}} \mathcal{L}^{th} \frac{\partial \boldsymbol{\tau}}{\partial \vartheta} \right) : \operatorname{sym} \frac{\partial \boldsymbol{v}}{\partial \mathbf{x}} + 2 \operatorname{sym} \left(\boldsymbol{\tau} : \frac{\partial \boldsymbol{v}}{\partial \mathbf{x}} \right) \\
&\quad - \frac{1}{T_m} \left\langle \Phi \left(\frac{f}{\kappa} - 1 \right) \right\rangle - \left[\left(\mathcal{L}^e + \frac{\chi^*}{\rho c_p} \mathcal{L}^{th} \boldsymbol{\tau} + \mathbf{g}\boldsymbol{\tau} + \boldsymbol{\tau}\mathbf{g} + \mathcal{W} \right) : \mathbf{P} \right] - \frac{\chi^{**} \Xi}{\rho c_p} \mathcal{L}^{th}, \\
\dot{\boldsymbol{\alpha}} &= 2 \operatorname{sym} \left(\boldsymbol{\alpha} : \frac{\partial \boldsymbol{v}}{\partial \mathbf{x}} \right) + \frac{1}{T_m} \left\langle \Phi \left(\frac{f}{\kappa} - 1 \right) \right\rangle \left[r_1(\xi, \vartheta) \, \mathbf{P} + r_2(\xi, \vartheta) \frac{\mathbf{P} : \mathbf{Q}}{\tilde{\boldsymbol{\tau}} : \mathbf{Q}} \tilde{\boldsymbol{\tau}} \right], \\
\dot{\xi} &= \Xi, \\
\dot{\vartheta} &= \frac{\vartheta}{c_p \rho_{Ref}} \frac{\partial \boldsymbol{\tau}}{\partial \vartheta} : \operatorname{sym} \frac{\partial \boldsymbol{v}}{\partial \mathbf{x}} + \frac{1}{T_m} \left\langle \Phi \left(\frac{f}{\kappa} - 1 \right) \right\rangle \frac{\chi^*}{c_p} \boldsymbol{\tau} : \mathbf{P} + \frac{\chi^{**}}{c_p} \Xi;
\end{aligned}
\tag{70}
$$

(ii) the boundary conditions

(a) displacement ϕ is prescribed on a part ∂_ϕ of $\partial\phi(\mathcal{B})$ and tractions $(\boldsymbol{\tau} \cdot \mathbf{n})^a$ are prescribed on part $\partial_{\boldsymbol{\tau}}$ of $\partial\phi(\mathcal{B})$, where $\partial_\phi \cap \partial_{\boldsymbol{\tau}} = 0$ and $\overline{\partial_\phi \cup \partial_{\boldsymbol{\tau}}} = \partial\phi(\mathcal{B})$;

(b) heat flux $\mathbf{q} \cdot \mathbf{n} = 0$ is prescribed on $\partial\phi(\mathcal{B})$;

(iii) the initial conditions

ϕ, $\boldsymbol{v}$, ρ, $\boldsymbol{\tau}$, $\boldsymbol{\alpha}$, ξ and ϑ are given at each particle $X \in \mathcal{B}$ at $t = 0$;

are satisfied.

5.2. Basic features of rate dependent plastic model

Rate dependency (viscosity) allows the spatial difference operator in the governing equations to retain its ellipticity and the initial value probleem (the Cauchy problem) is well-posed. Viscosity introduces implicitly a length-scale parameter into the dynamical innitial-boundary value problem.

The theory of viscoplasticity gives the possibility to obtain mesh-insensitive results.

Since the rate independent plastic response is obtained as the limit case when the relaxation time is equal to zero hence the theory of viscoplasticity offers the regularization procedure for the solution of dynamical initial-boundary value problems under cyclic loadings. Due to that we can investigate numerically the localized fatigue damage.

6. Numerical solution of the initial-boundary value problem (evolution problem)

6.1. Formulation of the evolution problem

Find φ as function of t and $\mathbf{x}$ satisfying[5]

$$\left.\begin{array}{ll} \text{(i)} & \dot{\varphi} = \mathcal{A}(t,\varphi)\varphi + \mathbf{f}(t,\varphi); \\ \text{(ii)} & \varphi(0) = \varphi^0(\mathbf{x}); \\ \text{(iii)} & \text{The boundary conditions} \\ & \text{(e.g. as have been postulated in Sec. 5.1),} \end{array}\right\} \tag{71}$$

where the unknown φ takes values in a Banach space, $\mathcal{A}(t,\varphi)$ is a spatial linear differential operator (in general unbounded) depending on t and φ, and $\mathbf{f}$ is a nonlinear function.

The evolution problem (71) describes an adiabatic inelastic flow process formulated in Sec. 5.1 provided

$$\varphi = \begin{bmatrix} \phi \\ \boldsymbol{v} \\ \rho \\ \boldsymbol{\tau} \\ \boldsymbol{\alpha} \\ \xi \\ \vartheta \end{bmatrix}, \qquad \mathbf{f} = \begin{bmatrix} \boldsymbol{v} \\ 0 \\ 0 \\ -\frac{1}{T_m}\left\langle \Phi\left(\frac{f}{\kappa}-1\right)\right\rangle \left[\left(\mathcal{L}^e + \frac{\chi^*}{\rho c_p}\mathcal{L}^{th}\boldsymbol{\tau} + \mathbf{g}\boldsymbol{\tau} + \boldsymbol{\tau}\mathbf{g} + \mathcal{W}\right) : \mathbf{P}\right] - \frac{\chi^{**}\Xi}{\rho c_p}\mathcal{L}^{th} \\ \frac{1}{T_m}\left\langle \Phi\left(\frac{f}{\kappa}-1\right)\right\rangle \left[r_1(\xi,\vartheta)\mathbf{P} + r_2(\xi,\vartheta)\frac{\mathbf{P}:\mathbf{Q}}{\boldsymbol{\tau}:\mathbf{Q}}\tilde{\boldsymbol{\tau}}\right] \\ \Xi \\ \frac{1}{T_m}\left\langle \Phi\left(\frac{f}{\kappa}-1\right)\right\rangle \frac{\chi^*}{\rho c_p}\boldsymbol{\tau} : \mathbf{P}\frac{\chi^{**}}{\rho c_p}\Xi \end{bmatrix},$$

$$\mathcal{A} = \begin{bmatrix} 0 & 0 & 0 & 0 & 0 & 0 & 0 \\ 0 & 0 & \frac{\boldsymbol{\tau}}{\rho_{Ref}\rho}\,\mathrm{grad} & \frac{1}{\rho_{Ref}}\,\mathrm{div} & 0 & 0 & 0 \\ 0 & -\rho\mathrm{div} & 0 & 0 & 0 & 0 & 0 \\ 0 & \mathbb{E} : \mathrm{sym}\frac{\partial}{\partial \mathbf{x}} + 2\,\mathrm{sym}(\boldsymbol{\tau} : \frac{\partial}{\partial \mathbf{x}}) & 0 & 0 & 0 & 0 & 0 \\ 0 & 2\,\mathrm{sym}(\boldsymbol{\alpha} : \frac{\partial}{\partial \mathbf{x}}) & 0 & 0 & 0 & 0 & 0 \\ 0 & 0 & 0 & 0 & 0 & 0 & 0 \\ 0 & \frac{\vartheta}{c_p\rho_{Ref}}\frac{\partial \boldsymbol{\tau}}{\partial \vartheta} : \mathrm{sym}\frac{\partial}{\partial \mathbf{x}} & 0 & 0 & 0 & 0 & 0 \end{bmatrix}, \tag{72}$$

where

$$\mathbb{E} = \mathcal{L}^e - \frac{\vartheta}{c_p\rho_{Ref}}\mathcal{L}^{th}\frac{\partial \boldsymbol{\tau}}{\partial \vartheta}.$$

It is noteworthy that the spatial operator $\mathcal{A}$ has the same form as in thermo-elastodynamics while all dissipative effects generated by viscoplastic flow phenomena influence the process through the nonlinear function $\mathbf{f}$.

[5]We shall follow here some fundamental results which have been discussed in Richtmyer and Morton [60], Strang and Fix [65], Hughes, Kato and Marsden [30], Richtmyer [59], Dautray and Lions [18], Gustafsson, Kreiss and Oliger [28] and Łodygowski and Perzyna [38, 39].

6.2. Strict solution of the evolution problem

A strict solution of (71) with $\mathbf{f}(t, \boldsymbol{\varphi}) \equiv 0$ (i.e. the homogeneous evolution problem) is defined as a function $\boldsymbol{\varphi}(t) \in \mathrm{E}$ (a Banach space) such that

$$\begin{aligned} &\boldsymbol{\varphi}(t) \in \mathcal{D}(\mathcal{A}), && \text{for all} \quad t \in [0, t_f], \\ &\lim_{\Delta t \to 0} \left\| \frac{\boldsymbol{\varphi}(t + \Delta t) - \boldsymbol{\varphi}(t)}{\Delta t} - \mathcal{A}\boldsymbol{\varphi}(t) \right\|_{\mathrm{E}} = 0 && \text{for all} \quad t \in [0, t_f]. \end{aligned} \tag{73}$$

The boundary conditions are taken care of by restricting the domain $\mathcal{D}(\mathcal{A})$ to elements of E that satisfy those conditions; they are assumed to be linear and homogeneous, so that the set $\mathbf{S}$ of all $\boldsymbol{\varphi}$ that satisfy them is a linear manifold; $\mathcal{D}(\mathcal{A})$ is assumed to be contained in $\mathbf{S}$.

The choice of the Banach space E, as well as the domain of $\mathcal{A}$, is an essential part of the formulation of the evolution problem.

6.3. Well-posedness of the evolution problem

The homogeneous evolution problem (i.e. for $\mathbf{f} \equiv 0$) is called well posed (in the sense of Hadamard) if it has the following properties (cf. Richtmyer [59] and Hughes et al. [30]):

(i) The strict solutions are uniquely determined by their initial elements;

(ii) The set Y of all initial elements of strict solutions is dense in the Banach space E;

(iii) For any finite interval $[0, t_0]$, $t_0 \in [0, t_f]$ there is a constant $K = K(t_0)$ such that every strict solution satisfies the inequality

$$\|\boldsymbol{\varphi}(t)\| \leq K \|\boldsymbol{\varphi}^0\|, \qquad \text{for} \quad 0 \leq t \leq t_0. \tag{74}$$

The inhomogeneous evolution problem (71) will be called well posed if it has a unique solution for all reasonable choices of $\boldsymbol{\varphi}^0$ and $\mathbf{f}(t, \boldsymbol{\varphi})$ and if the solution depends continuously, in some sense, on those choices.

It is evident that any solution is unique, because of the uniqueness of the solutions of the homogeneous evolution problem. Namely, the difference of two solutions, for given $\boldsymbol{\varphi}^0$ and given $\mathbf{f}(\cdot)$, is a solution of the homogeneous problem with zero as initial element, hence must be zero for all t.

It is possible to show (cf. Richtmyer [59]) that strict solutions exist for sets of $\boldsymbol{\varphi}^0$ and $\mathbf{f}(\cdot)$ that are dense in E and E_1 (a new Banach space), respectively.

Let $\{\mathbb{F}_t^*; t \geq 0\}$ be a semi-group generated by the operator $\mathcal{A} + \mathbf{f}(\cdot)$ and $\{\mathbb{F}_t; t \geq 0\}$ be a semi-group generated by the operator $\mathcal{A}$.

Then we can write the generalized solution of the nonhomogenous evolution problem (71) in alternative forms

$$\begin{aligned} \boldsymbol{\varphi}(t, \mathbf{x}) &= \mathbb{F}^*(t)\boldsymbol{\varphi}^0(\mathbf{x}) \\ &= \mathbb{F}(t)\boldsymbol{\varphi}^0(\mathbf{x}) + \int_0^t \mathbb{F}(t - s)\mathbf{f}(s, \boldsymbol{\varphi}(s))\mathrm{d}s. \end{aligned} \tag{75}$$

The generalized solution of the nonhomogeneous evolution problem (71) in the form $(75)_2$ is the integral equation.

The successive approximations for $(75)_2$ are defined to be the functions $\boldsymbol{\varphi}_0, \boldsymbol{\varphi}_1, \ldots$, given by the formulas

$$\begin{aligned} &\boldsymbol{\varphi}_0(t) \quad = \boldsymbol{\varphi}^0, \\ &\boldsymbol{\varphi}_{k+1}(t) = \mathbb{F}(t)\boldsymbol{\varphi}^0 + \int_0^t \mathbb{F}(t - s)\mathbf{f}(s, \boldsymbol{\varphi}_k(s))\,\mathrm{d}s, \qquad k = 0, 1, 2, \ldots; \qquad t \in [0, t_f]. \end{aligned} \tag{76}$$

It is possible to show that these functions actually exist on $t \in [0, t_f]$ if the continuous function $\mathbf{f}$ is Lipschitz continuous with respect to the second argument uniformly with respect to $t \in [0, t_f]$. Then $(75)_2$ has unique solution (cf. Ionescu and Sofonea [31]).

6.4. Discretisation in space and time

We must approximate (71) twice. First, when E is infinite dimensional, we must replace $\mathcal{A}$ by an operator $\mathcal{A}_h$ which operates in a finite dimensional space $V_h \subset \mathrm{E}$, where, in general, $h > 0$ represents a discretisation step in space, such that $\dim(V_h) \to \infty$ as $h \to 0$. Second, we must discretise in time, that is to say choose a sequence of moments t_n (for example $t_n = n\Delta t$, where Δt is time step) at which we shall calculate the approximate solution.

Let us introduce the following semi-discretised (discrete in space) problem.

$$\left.\begin{array}{ll} \text{Find} & \boldsymbol{\varphi}_h \in \mathcal{C}^0([0, t_0]; V_h) \\ & (\mathcal{C}^0 \text{ denotes the space of functions continuous on } ([0, t_0], V_h)) \\ \text{satisfying} & \dfrac{\mathrm{d}\boldsymbol{\varphi}_h(t)}{dt} = \mathcal{A}_h \boldsymbol{\varphi}_h(t) + \mathbf{f}_h(t), \\ & \boldsymbol{\varphi}_h(0) = \boldsymbol{\varphi}_{0,h}. \end{array}\right\} \tag{77}$$

The operator $\mathcal{A}_h$ for the finite difference method can be obtained by approximating the spatial derivatives by differential quotients using the values of $\boldsymbol{\varphi}_h$ over a grid of points.

The operator $\mathcal{A}_h$ for the finite element method can be determined by a variational formulation approach. The discrete equations are obtained by the Galerkin method at particular points in the domain.

Finally, we shall define a method allowing us to calculate $\boldsymbol{\varphi}_h^n \in V_h$, an approximation to $\boldsymbol{\varphi}_h(t_n)$ starting from $\boldsymbol{\varphi}_h^{n-1}$ (we limit ourselves to a two-level scheme). Then we can write

$$\boldsymbol{\varphi}_h^{n+1} = C_h(\Delta t)\boldsymbol{\varphi}_h^n + \Delta t \mathbf{f}_h^n, \qquad \boldsymbol{\varphi}_h^0 = \boldsymbol{\varphi}_{0,h}, \tag{78}$$

where we introduce the operator $C_h(\Delta t) \in \mathcal{L}(V_h)$ ($\mathcal{L}$ is the set of continuous linear mapping of V_h with values in V_h) and where $\mathbf{f}_h^n$ approximates $\mathbf{f}_h(t_n)$.

We shall always assume that the evolution problem (71) is well posed and there exists a projection R_h of E into V_h such that

$$\lim_{h \to 0} |R_h \boldsymbol{\varphi} - \boldsymbol{\varphi}|_{\mathrm{E}} = 0 \qquad \forall \boldsymbol{\varphi} \in \mathrm{E}. \tag{79}$$

6.5. Convergence, consistency and stability

The first fundamental question is that of the convergence, when h and Δt tend to zero, of the sequence $\{\boldsymbol{\varphi}_h^n\}$, the solution (78), towards the function $\boldsymbol{\varphi}(t)$, the solution of (71). Let us restrict our consideration, for the moment, to the case where $\mathbf{f}(t) \equiv 0$.

Definition 1. *The scheme defined by (78) will be called convergent if the condition*

$$\boldsymbol{\varphi}_{0,h} \to \boldsymbol{\varphi}^0 \quad \text{as} \quad h \to 0 \tag{80}$$

implies that

$$\boldsymbol{\varphi}_h^n \to \boldsymbol{\varphi}(t) \quad \text{as} \quad \Delta t \to 0, \quad n \to \infty \quad \text{with} \quad n\Delta t \to t \tag{81}$$

for all $t \in [0, t_0]$, $t_0 \in [0, t_f]$, where $\boldsymbol{\varphi}_h^n$ is defined by (78) and $\boldsymbol{\varphi}(t)$ is the solution of (71). All this holds for arbitrary $\boldsymbol{\varphi}^0$.

The study of the convergence of an approximation scheme involves two fundamental properties of the scheme, consistency and stability.

Definition 2. *The scheme defined by (78) is called stable, if there exists a constant* $K \geq 1$ *independent of* h *and* Δt *such that*

$$\|(C_h(\Delta t))^n R_h\|_{\mathcal{L}(\mathrm{E})} \leq K \quad \forall n, \Delta t \qquad \text{satisfying} \quad n\Delta t \leq t_0 \,. \tag{82}$$

In the Definitions 1 and 2 there occur two parameters h and Δt. It may be that the scheme is not stable (or convergent) unless Δt and h satisfy supplementary hypotheses of the type $\Delta t/h^\alpha \leq$ constant, $\alpha < 0$, in which case we call the scheme **conditionally stable**. If the scheme is stable for arbitrary h and Δt we say that it is **unconditionally stable**.

Definition 3. *The scheme defined by (78) will be called consistent with equation (71) if there exists a subspace* $Y \subset \mathrm{E}$ *dense in* E, *such that for every* $\varphi(t)$ *which is a solution of (71) with* $\varphi^0 \subset Y$ *(and* $\mathbf{f} \equiv 0$*) we have*

$$\lim_{h\to 0,\ \Delta t\to 0} \left| \frac{C_h(\Delta t) R_h \varphi(t) - \varphi(t)}{\Delta t} - A\varphi(t) \right|_{\mathrm{E}} = 0. \tag{83}$$

6.6. Application of the finite difference method

Let us consider the evolution problem in the form of (71). Let us introduce in the Euclidean space E^3 a regular difference net of nodes (i,j,k) with convective coordinates $\chi_i^1 = i\Delta\chi^1$, $\chi_j^2 = j\Delta\chi^2$ and $\chi_k^3 = k\Delta\chi^3$, $i,j,k \in N$, where N is a set of natural numbers, cf. Dornowski [19]. Of course, some of the nodes belong to the edge of the body and are used to approximate the boundary conditions. Time is approximated by a discrete sequence of moments $t_n = n\Delta t$, where Δt is time step, $n \in N$.

For all functions $\varphi = \hat{\varphi}(\mathbf{x}, t)$ of the analysed problem we postulate the following approximation in the domain $\Delta\mathrm{E} = \Delta\chi^1 \times \Delta\chi^2 \times \Delta\chi^3$ of a convective difference mesh (cf. Fig. 5):

$$\begin{aligned}\varphi(\mathbf{x},t) \cong \varphi_h(\mathbf{x},t) = {} & \mathbf{a}_1(t) + \mathbf{a}_2(t)\chi^1 + \mathbf{a}_3(t)\chi^2 + \mathbf{a}_4(t)\chi^3 \\ & + \mathbf{a}_5(t)\chi^1\chi^2 + \mathbf{a}_6(t)\chi^1\chi^3 + \mathbf{a}_7(t)\chi^2\chi^3 + \mathbf{a}_8(t)\chi^1\chi^2\chi^3, \qquad \mathbf{x} \in \Delta\mathcal{S}.\end{aligned} \tag{84}$$

The functions $\mathbf{a}_1(t), \ldots, \mathbf{a}_8(t)$ depend only on time, are determined by the value of the function $\varphi_w(t) = [\varphi_1(t), \ldots, \varphi_8(t)]^T$ in the node points of difference mesh, (cf. Fig. 5). Hence the approximation functions (84) can be written in the form

$$\varphi_h(\mathbf{x},t) = \mathbf{N}(\mathbf{x})\varphi_w(t), \qquad \mathbf{x} \in \Delta\mathcal{S}, \tag{85}$$

where

$$\begin{aligned}
N_1(\mathbf{x}) &= \overline{\chi}\,(-\Delta\chi^1 + 2\chi^1)\,(-\Delta\chi^2 + 2\chi^2)\,(\Delta\chi^3 - 2\chi^3)\,, \\
N_2(\mathbf{x}) &= \overline{\chi}\,(\Delta\chi^1 + 2\chi^1)\,(-\Delta\chi^2 + 2\chi^2)\,(-\Delta\chi^3 + 2\chi^3)\,, \\
N_3(\mathbf{x}) &= \overline{\chi}\,(-\Delta\chi^1 + 2\chi^1)\,(\Delta\chi^2 + 2\chi^2)\,(-\Delta\chi^3 + 2\chi^3)\,, \\
N_4(\mathbf{x}) &= \overline{\chi}\,(\Delta\chi^1 + 2\chi^1)\,(\Delta\chi^2 + 2\chi^2)\,(\Delta\chi^3 - 2\chi^3)\,, \\
N_5(\mathbf{x}) &= \overline{\chi}\,(-\Delta\chi^1 + 2\chi^1)\,(-\Delta\chi^2 + 2\chi^2)\,(\Delta\chi^3 + 2\chi^3)\,, \\
N_6(\mathbf{x}) &= \overline{\chi}\,(\Delta\chi^1 + 2\chi^1)\,(\Delta\chi^2 - 2\chi^2)\,(\Delta\chi^3 + 2\chi^3)\,, \\
N_7(\mathbf{x}) &= \overline{\chi}\,(\Delta\chi^1 - 2\chi^1)\,(\Delta\chi^2 + 2\chi^2)\,(\Delta\chi^3 + 2\chi^3)\,, \\
N_8(\mathbf{x}) &= \overline{\chi}\,(\Delta\chi^1 + 2\chi^1)\,(\Delta\chi^2 + 2\chi^2)\,(\Delta\chi^3 + 2\chi^3)\,, \\
\overline{\chi} &= \frac{1}{8\Delta\chi^1\Delta\chi^2\Delta\chi^3}\,.
\end{aligned} \tag{86}$$

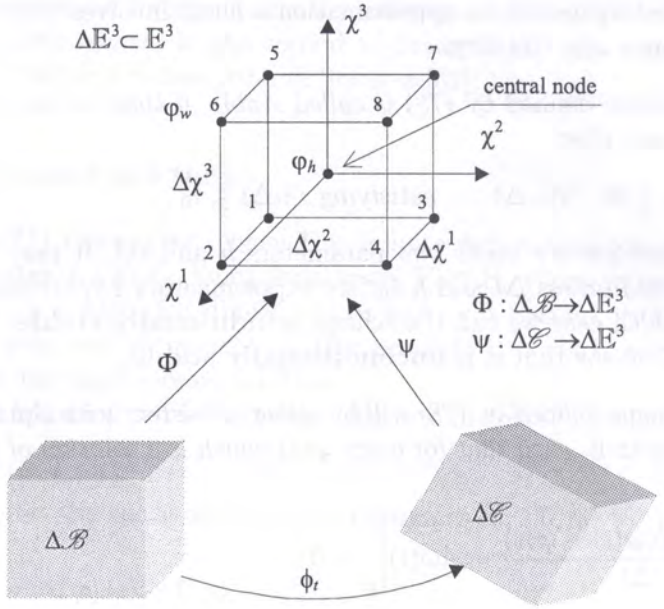

Fig. 5. Convective finite difference mesh of nodes

Equations (85) allow to determine values of the function $\varphi_h(\mathbf{x},t)$ in any point of the difference mesh, $\mathbf{x} \in \Delta\mathcal{S}$. For the central point $\mathbf{x} = \mathbf{x}_0$, $N_1 = \cdots = N_8 = \frac{1}{8}$ and $\varphi_h(t) = [\varphi_1(t) + \ldots + \varphi_8(t)]\frac{1}{8}$.

By using (85) we can determine the matrix of the difference operators which approximate the first partial derivatives of the function $\varphi(\mathbf{x},t)$ for $\mathbf{x} \in \Delta\mathcal{S}$,

$$\frac{\partial}{\partial \mathbf{x}}\varphi(\mathbf{x},t) \cong \frac{\partial}{\partial \mathbf{x}}\varphi_h(\mathbf{x},t) = \frac{\partial}{\partial \mathbf{x}}\mathbf{N}(\mathbf{x})\varphi_w(t) = \mathbf{R}(\mathbf{x})\varphi_w(t). \tag{87}$$

The matrix of the difference operator $\mathbf{R}(\mathbf{x})$ for the central point takes the form

$$\mathbf{R}(\mathbf{x}=\mathbf{x}_0) = \frac{\partial}{\partial \mathbf{x}}\mathbf{N}(\mathbf{x})\Big|_{\mathbf{x}=\mathbf{x}_0} = \begin{bmatrix} \frac{-1}{\Delta\chi^1} & \frac{1}{\Delta\chi^1} & \frac{-1}{\Delta\chi^1} & \frac{1}{\Delta\chi^1} & \frac{-1}{\Delta\chi^1} & \frac{1}{\Delta\chi^1} & \frac{-1}{\Delta\chi^1} & \frac{1}{\Delta\chi^1} \\ \frac{-1}{\Delta\chi^2} & \frac{-1}{\Delta\chi^2} & \frac{1}{\Delta\chi^2} & \frac{1}{\Delta\chi^2} & \frac{-1}{\Delta\chi^2} & \frac{-1}{\Delta\chi^2} & \frac{1}{\Delta\chi^2} & \frac{1}{\Delta\chi^2} \\ \frac{-1}{\Delta\chi^3} & \frac{-1}{\Delta\chi^3} & \frac{-1}{\Delta\chi^3} & \frac{-1}{\Delta\chi^3} & \frac{1}{\Delta\chi^3} & \frac{1}{\Delta\chi^3} & \frac{1}{\Delta\chi^3} & \frac{1}{\Delta\chi^3} \end{bmatrix}. \tag{88}$$

In similar way we can find the difference form of the spatial difference operator $\mathcal{A}(t,\varphi)$ of the considered evolution problem (71)

$$\mathcal{A}(t,\varphi)\varphi \cong \mathcal{A}(t,\varphi_h)\mathbf{N}(\mathbf{x})\varphi_w(t) = \mathcal{A}_h(t,\varphi_h)\varphi_w(t), \tag{89}$$

hence

$$\mathcal{A}_h(t,\varphi_h) = \mathcal{A}(t,\varphi_h)\mathbf{N}(\mathbf{x}) \qquad \text{for} \quad \mathbf{x} \in \Delta\mathcal{S}. \tag{90}$$

For the central node, $\mathbf{x} = \mathbf{x}_0$ the difference operator (90) depends only on time.

As a result of the proposed approximation of the evolution problem (71) with respect to the spatial variables we obtain a set of differential equations with respect to time and difference equations with respect to spatial variables

$$\frac{\mathrm{d}\,\varphi_h(t)}{\mathrm{d}t} = \mathcal{A}_h\varphi_w(t) + \mathbf{f}_h(t). \tag{91}$$

For the approximation of (91) with respect to time we use the evident scheme of the first order in the form

$$\frac{\mathrm{d}\,\varphi_h(t)}{\mathrm{d}t} \cong \frac{\varphi_h^{n+1} - \varphi_h^n}{\Delta t} = \mathcal{A}_h\varphi_w^n + \mathbf{f}_h^n. \tag{92}$$

The solution of (92) is reduced to the realization of the recurrence relation

$$\varphi_h^{n+1} = C_h(\Delta t)\varphi_w^n + \Delta t \mathbf{f}_h^n . \tag{93}$$

The difference operator

$$C_h(\Delta t) = \Delta t \mathcal{A}_h + \mathbf{N} \tag{94}$$

couple dependent variables and various points of difference mesh.

For the finite difference approximation it can be proved that the introduced scheme (93) is consistent with equation (71).

6.7. Stability criterion

In explicit finite difference scheme for a set of the partial differential equations (71)(i) of the hiperbolic type the condition of stability is the criterion of Courant–Friedrichs–Lewy, cf. Courant et al. [9]

$$\Delta t_{n,n+1} \leq \min \left(\frac{\Delta L_{p,q,r}^n}{|c_{p,q,r}^n|} \right), \qquad p = 1,2,3,\ldots,P; \quad q = 1,2,3,\ldots,Q; \quad r = 1,2,3,\ldots,R, \tag{95}$$

where $\Delta t_{n,n+1}$ denotes time step, $c_{p,q,r}^n$ denotes the velocity of the propagation of the disturbances in the vicinity of the central node (p,q,r), $\Delta L_{p,q,r}^n$ is the minimum distance between the mesh nodes which are in the vicinity of the node (cf. Fig. 5).

The Courant–Friedrichs–Lewy condition requires that the numerical domain of dependence of a finite-difference scheme include the domain of dependence of the associated partial differential equations, cf. Durran [23].

6.8. The Lax–Richtmyer equivalence theorem

We can now state the Lax–Richtmyer equivalence theorem (cf. Richtmyer and Morton [60], Strang and Fix [65], Dautray and Lions [18] and Gustafsson, Kreiss and Oliger [28]).

Theorem 1. *Suppose that the evolution problem (71) is well-posed for $t \in [0, t_0]$ and that it is approximated by the scheme (93), which we assume consistent. Then the scheme is convergent if and only if it is stable.*

The proof of the Lax–Richtmyer equivalence theorem for the case when the partial differential operator $\mathcal{A}$ in (71) is independent of φ can be found in Dautray and Lions [18].

Remark. Let us consider the evolution problem (71) with

$$\mathbf{f}(t,\varphi) \neq 0 \tag{96}$$

and $\varphi^0 = 0$, and also the corresponding approximation (93). We have

$$\varphi_h^{n+1} = \Delta t \sum_{j=1}^{n} [C_h(\Delta t)]^{n-j} \mathbf{f}_h^j . \tag{97}$$

If $\mathcal{A}$ is the infinitesimal generator of a semigroup $\{\mathbb{F}(t)\}$ we can write

$$\varphi(t) = \int_0^t \mathbb{F}(t-s)\mathbf{f}(s)\,\mathrm{d}s. \tag{98}$$

Under suitable hypotheses on the convergence of $\mathbf{f}_h^j$ to $\mathbf{f}(j\Delta t)$ we can show that expression (97) converges to (98) if the scheme is stable and consistent.

7. IDENTIFICATION PROCEDURE

7.1. Assumptions of the material functions

The plastic potential function f is assumed in the form (cf. Perzyna [51] and Shima and Oyane [62])

$$f = \left\{ \tilde{J}_2' + [n_1(\vartheta) + n_2(\vartheta)\xi]\, \tilde{J}_1^2 \right\}^{\frac{1}{2}} \tag{99}$$

where

$$n_1(\vartheta) = 0, \qquad n_2(\vartheta) = \text{const.} \tag{100}$$

The isotropic work-hardening-softening function κ is postulated as (cf. Perzyna [52, 53] and Nemes and Eftis [46])

$$\kappa = \hat{\kappa}(\epsilon^p, \vartheta, \xi) = \{\kappa_s(\vartheta) - [\kappa_s(\vartheta) - \kappa_0(\vartheta)] \exp[-\delta(\vartheta)\epsilon^p]\} \left[1 - \left(\frac{\xi}{\xi_F}\right)^{\beta(\vartheta)}\right], \tag{101}$$

where

$$\begin{aligned} &\kappa_s(\vartheta) = \kappa_s^* - \kappa_s^{**}\overline{\vartheta}, \qquad \kappa_0(\vartheta) = \kappa_0^* - \kappa_0^{**}\overline{\vartheta}, \\ &\delta(\vartheta) = \delta^* - \delta^{**}\overline{\vartheta}, \qquad \beta(\vartheta) = \beta^* - \beta^{**}\overline{\vartheta}, \qquad \overline{\vartheta} = \frac{\vartheta - \vartheta_0}{\vartheta_0}. \end{aligned} \tag{102}$$

The overstress function $\Phi\left(\frac{f}{\kappa} - 1\right)$ is assumed in the form

$$\Phi\left(\frac{f}{\kappa} - 1\right) = \left(\frac{f}{\kappa} - 1\right)^m. \tag{103}$$

The evolution equation for the kinematic hardening parameter $\boldsymbol{\alpha}$ is assumed in the form (59) with

$$\zeta_1(\xi, \vartheta) = \zeta_1^* - \zeta_1^{**}\overline{\vartheta}, \qquad \zeta_2(\xi, \vartheta) = \zeta_2^* - \zeta_2^{**}\overline{\vartheta}. \tag{104}$$

The evolution equation for the porosity ξ is postulated as

$$\dot{\xi} = \dot{\xi}_{grow} = \frac{g^*(\xi, \vartheta)}{T_m \sqrt{\kappa_0(\vartheta)}} \left[\tilde{I}_g - \tau_{eq}(\xi, \vartheta, \epsilon^p)\right] \tag{105}$$

where (cf. Dornowski [19])

$$\begin{aligned} g^*(\xi, \vartheta) &= c_1(\vartheta) \frac{\sqrt{\kappa_0(\vartheta)}}{\kappa_0(\vartheta)} \frac{\xi}{1 - \xi}, \\ \tilde{I}_g &= b_1 \tilde{J}_1 + b_2 \sqrt{\tilde{J}_2}, \\ \tau_{eq}(\xi, \vartheta, \epsilon^p) &= c_2(\vartheta)(1 - \xi) \ln \frac{1}{\xi} \{2\kappa_s(\vartheta) - [\kappa_s(\vartheta) - \kappa_0(\vartheta)]\, F(\xi_0, \xi, \vartheta)\}, \\ &\qquad c_1(\vartheta) = \text{const}, \quad c_2(\vartheta) = \text{const}, \\ F(\xi_0, \xi, \vartheta) &= \left(\frac{\xi_0}{1 - \xi_0} \frac{1 - \xi}{\xi}\right)^{\frac{2}{3}\delta} + \left(\frac{1 - \xi}{1 - \xi_0}\right)^{\frac{2}{3}\delta}. \end{aligned} \tag{106}$$

As in the infinitesimal theory of elasticity we assume linear properties of the material, i.e.

$$\mathcal{L}^e = 2\mu \mathbf{I} + \lambda(\mathbf{g} \otimes \mathbf{g}) \tag{107}$$

where μ and λ denote the Lamé constants, and the thermal expansion matrix is postulated as

$$\mathcal{L}^{th} = (2\mu + 3\lambda)\theta \mathbf{g}, \tag{108}$$

where θ is the thermal expansion constant.

To identify the material function η^* in the evolution equation

$$\boldsymbol{\omega}^P = \eta^* \Lambda(\boldsymbol{\alpha} \cdot \mathbf{P} - \mathbf{P} \cdot \boldsymbol{\alpha}) \tag{109}$$

we assume that the value of plastic spin is the same order of magnitude as the value of the rate of plastic deformation. This proposition was first introduced by Khan and Cheng [34]. It gives

$$\eta^* = \frac{1}{[(\boldsymbol{\alpha} \cdot \mathbf{P} - \mathbf{P} \cdot \boldsymbol{\alpha}) : (\boldsymbol{\alpha} \cdot \mathbf{P} - \mathbf{P} \cdot \boldsymbol{\alpha})]^{1/2}} \,. \tag{110}$$

7.2. Identification of the material constants

To determine the material constants assumed in Sec. 7.1 we take advantage of the experimental observations presented by Chakrabarti and Spretnak [7]. They investigated the localized fracture mode for tensile steel sheet specimens simulating both plane stress and plane strain processes. The material used in their study was AISI 4340 steel. The principal variable in this flat specimen test was the width-to-thickness ratio. Variation in specimen geometry produces significant changes in stress state, directions of shear bands, and ductility. They found that fracture propagated consistently along the shear band localized region.

Let us now consider the adiabatic dynamic process for a thin steel plate under condition of plane stress state. In fact we idealize the initial-boundary value problem investigated by Chakrabarti and Spretnak [7] by assuming the velocity driven adiabatic process for a thin steel plate. Dimensions of the plate and the variation in time of the kinematic constraints are presented in Fig. 6. The problem has been solved by using the finite difference method. A thin sheet is modelled via $N \times M$ elements, cf. Fig. 6.

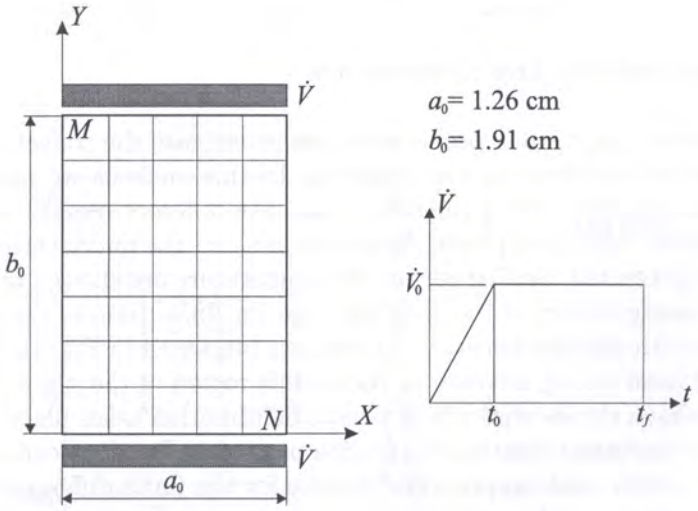

Fig. 6. Dimension of the plate and the variation in time of the kinematic constrains (After Chakrabarti and Spretnak [7])

In numerical calculations it is assumed:

$$\dot{V}_0 = 1.5 \text{ m/s}, \qquad t_0 = 50 \ \mu\text{s}, \qquad t_f = 800 \ \mu\text{s}.$$

The material of a plate is AISI 4340 steel.

Based on the best curve fitting of the experimental results obtained by Chakrabarti and Spretnak [7] for the stress-strain relation (cf. Fig. 7) the identification of the material constants has been done, cf. Table 2.

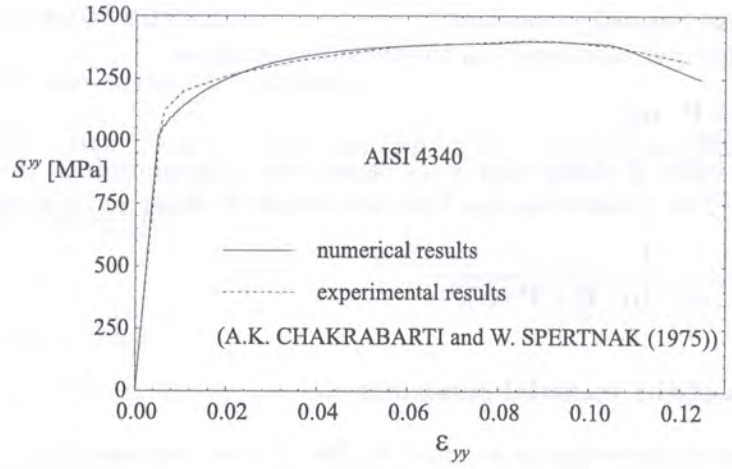

Fig. 7. Component S^{YY} of the second Piola–Kirchhoff stress tensor as a function of the logarithmic strain ε_{YY}

Table 2. Material constants for AISI 4340 steel

$\kappa_s^* = 809$ MPa	$\kappa_s^{**} = 228$ MPa	$\kappa_0^* = 598$ MPa	$\kappa_0^{**} = 168$ MPa
$\delta^* = 14.00$	$\delta^{**} = 3.94$	$\beta^* = 9.00$	$\beta^{**} = 2.53$
$\vartheta_0 = 293$ K	$\xi_F = 0.20$	$\rho_{Ref} = 7850$ kg/m^3	$\mu = 76.92$ GPa
$\lambda = 115.38$ GPa	$\theta = 12 \cdot 10^{-6}$ K^{-1}	$T_m = 2.5$ ms	$m = 1$
$\zeta_1^* = 15.00$ GPa	$\zeta_1^{**} = 4.22$ GPa	$\zeta_2^* = 69.60$	$\zeta_2^{**} = 19.60$
$c_1 = 0.202$	$c_2 = 6.7 \cdot 10^{-2}$	$b_1 = 1.00$	$b_2 = 1.30$
$\xi_0 = 6 \cdot 10^{-4}$	$\overline{\chi} = 0.85$	$\overline{\overline{\chi}} = 0$	$c_p = 455$ J/kg K

7.3. Investigation of stability and convergence

Using the same initial-boundary value problem we can investigate the convergence of the numerical method based on the finite difference discretization. In this analysis we assume that the micro-damage evolution is investigated. For a thin steel plate five different meshes have been assumed. In Fig. 8 distributions of the equivalent plastic deformation along the middle cross-section ($X = a_0/2$) for various meshes are presented. Similar results for temperature are showed in Fig. 9. All curves are plotted in the initial configuration of the specimen and for finite time of the process, $t_f = 800$ μs. The deformed meshes with various densities of nodes are presented in Fig. 10. Both analysed values shown in Fig. 8 and 9 have strong increase in the middle region of the plate. This suggests that in that region of the specimen the localization of plastic deformation takes place. Based on the results for distributions of the equivalent plastic deformation plotted in Fig. 8 we can observe that the finite width of the localized region needs appropriate density for the finite difference mesh (in considered case higher than 864 nodes).

The numerical procedure for the explicit finite difference scheme (93) has been accomplished with various time step Δt. The value of the time step has been determined by using the stability criterion (95). In Fig. 11 the evolution of the time step Δt in the deformation process for the mesh $N \times M = 3456$ has been shown. For the considered deformation process the time step Δt is decreasing function of time.

The stability of the numerical procedure with constant time step can be keeping in entire interval $[0, t_f]$ provided we assume $\Delta t = 0.025$ μs. Then as a result for the considered deformation process we have 32 000 time steps. While the analogical process with various time step Δt is accomplished for 26 603 time steps. This decreases very much time of computation. Very intense change of time step Δt observed from $t = 0.6$ ms in Fig. 11 is caused by the formation of the shear band localization.

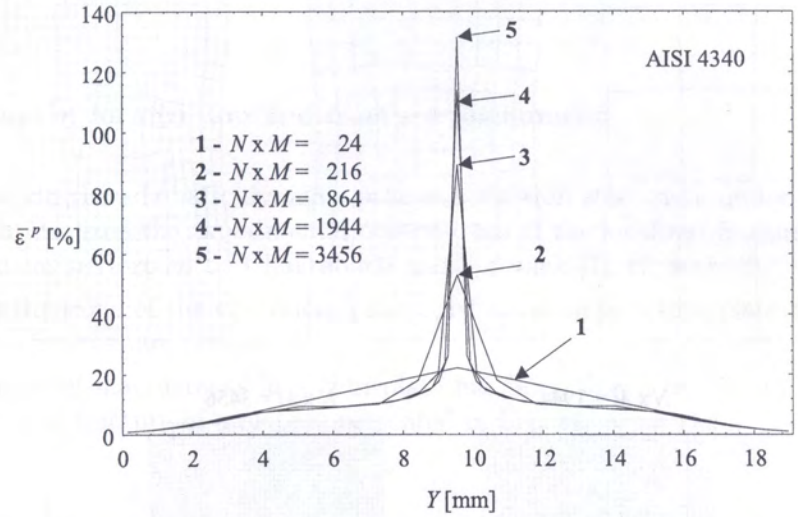

Fig. 8. Distributions of the equivalent plastic deformation along the middle cross-section ($X = a_0/2$) for various meshes

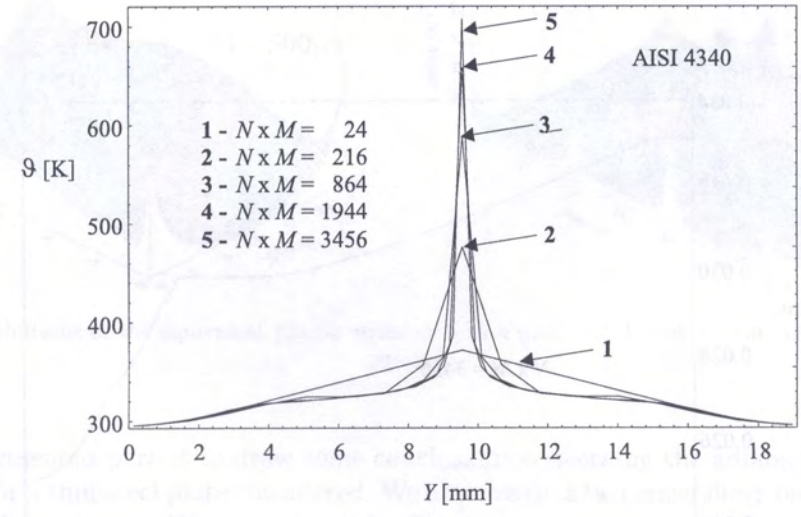

Fig. 9. Distributions of the temperature along the the middle cross-section ($X = a_0/2$) for various meshes

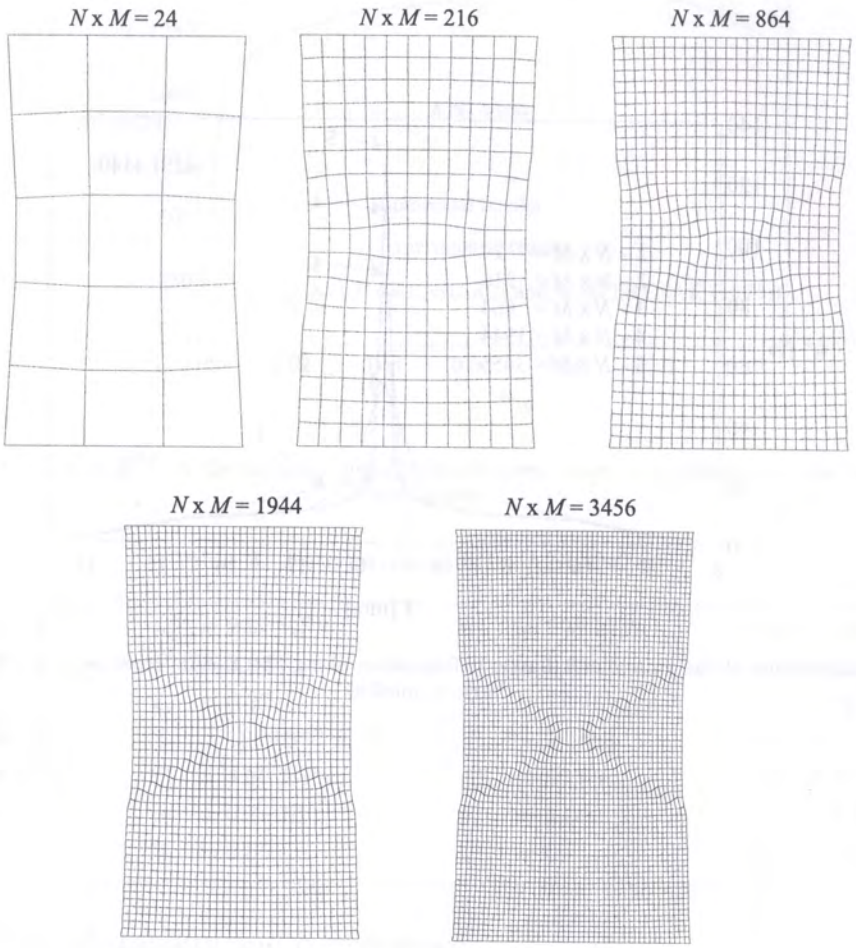

Fig. 10. Deformed meshes with various densities of nodes

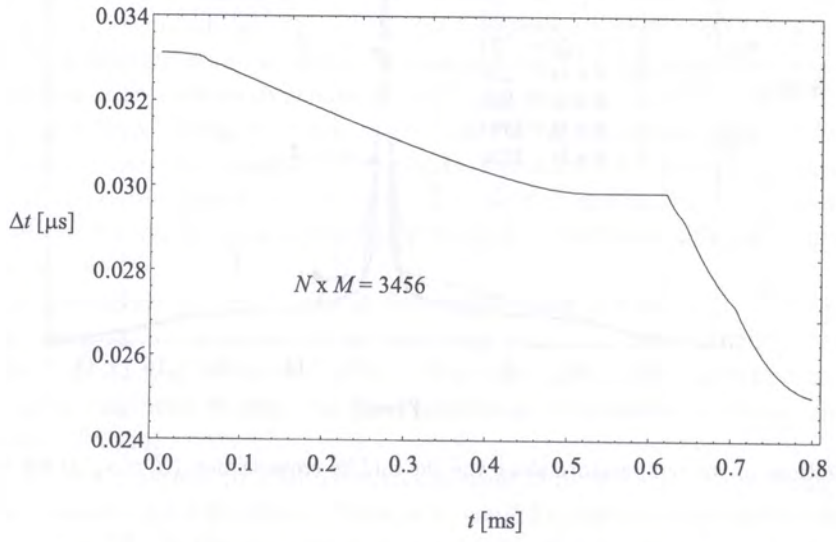

Fig. 11. Evolution of the time step Δt for a mesh with 3456 nodes

The results obtained show that the satisfaction of the stability criterion (95) leads to the convergence of the numerical procedure. We can conclude that the assumed finite difference scheme (93) approximates the well posed initial-boundary value problem (71). These results can be treated as the numerical proof of the Lax–Richtmyer equivalence theorem formulated in Sec. 6.8.

7.4. Investigation of localization and fracture phenomena

Let us consider again the adiabatic dynamic process for a thin steel plate under condition of plane stress state which idealized the experimental observations of the localized fracture mode for tensile steel sheet specimens performed by Chakrabarti and Spretnak [7], cf. Sec. 7.2.

In Fig. 12 distributions of the equivalent plastic deformation in a thin plate for chosen instants of the deformation process are presented.

The development of macrocracks in a thin plate has been shown in Fig. 13 and the deformed configuration for final fracture of a plate is presented in Fig. 14.

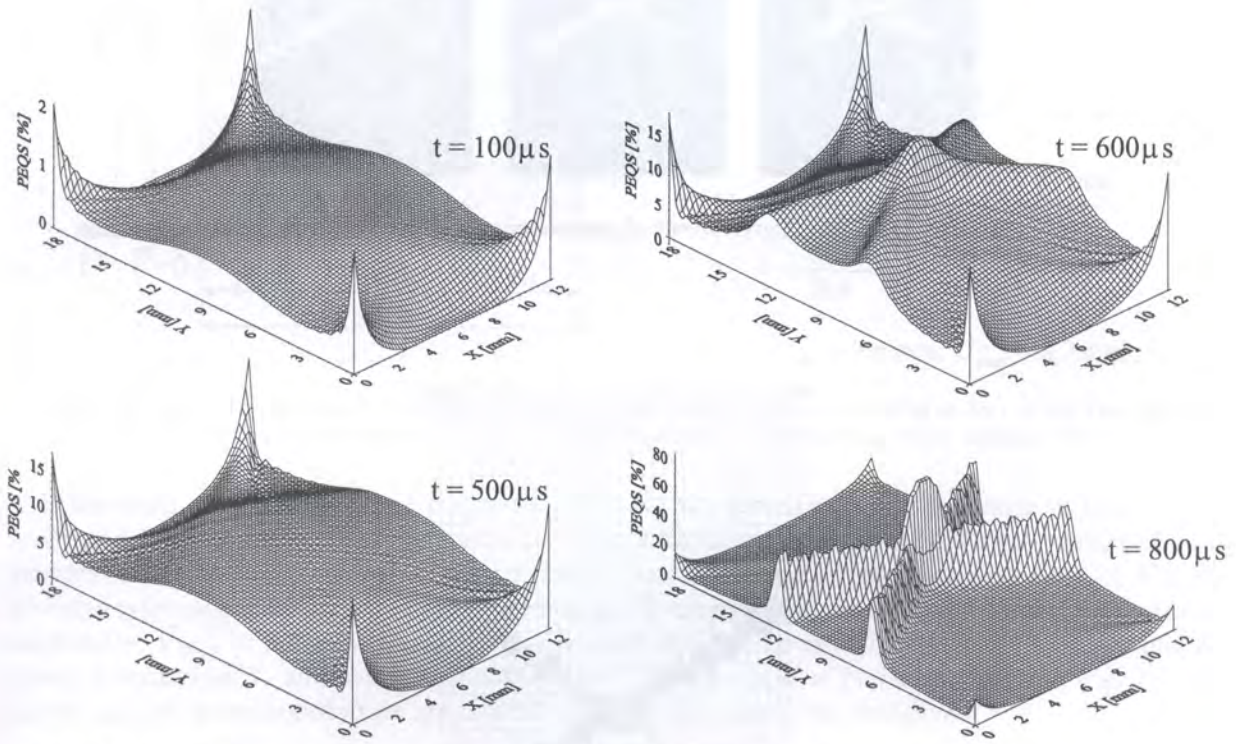

Fig. 12. Distributions of the equivalent plastic strain in a thin plate for chosen instants of the deformation process

The results presented permit to draw some conclusions concerning the adiabatic dynamic deformation process for a thin steel plate considered. We observe that two cross shear bands are developed in the center of the specimen. With continued loading process, one of the instability bands becomes more predominant and most of the plastic deformation is confirmed to this particular adiabatic shear band. Fracture occurs along the boundary of this active instability band. The symmetry breaking in the deformation process observed is only due to very small imperfections generated by numerical procedure. The obtained results are in accord with the experimental observations of Chakrabarti and Spretnak [7].

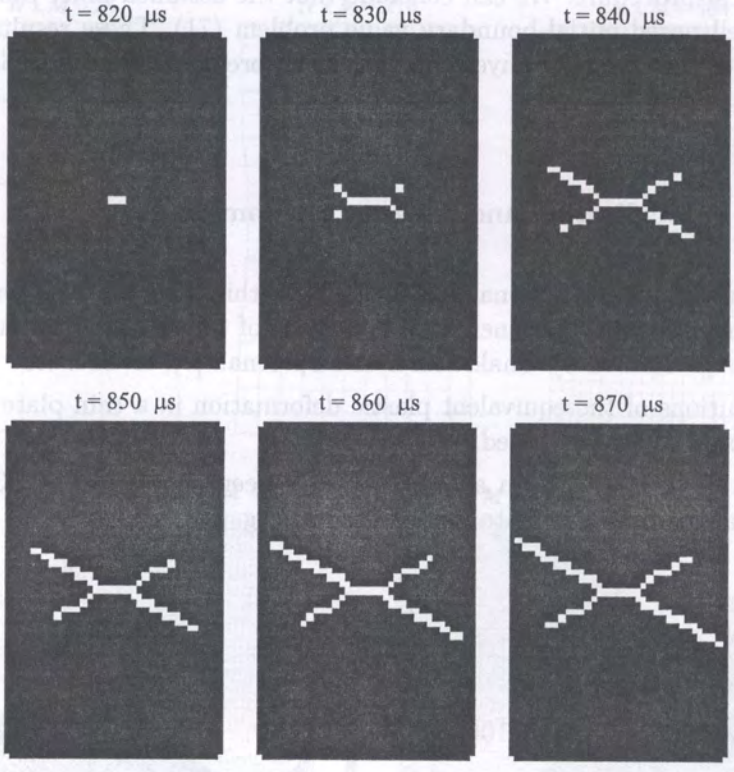

Fig. 13. Development of macrocracks in a thin plate

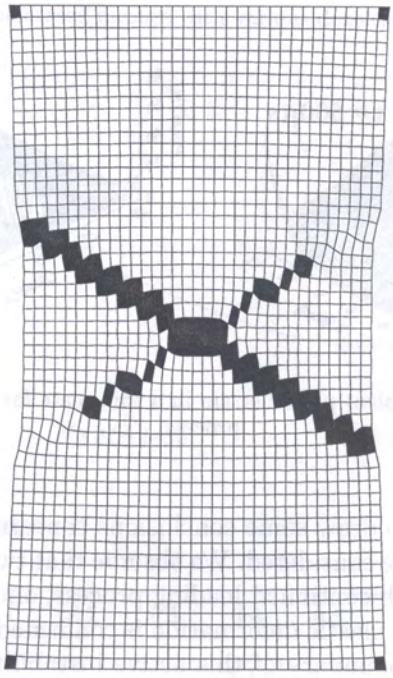

Fig. 14. Deformed configuration for final fracture of the plate

8. Particular examples

8.1. Dynamic adiabatic and isothermal, cyclic loading processes for a thin plate with small rectangular hole

Let us consider dynamic, adiabatic and isothermal, cyclic loading processes for a thin steel plate with small rectangular hole located in the centre. To the upper edge of the plate the normal and parallel displacements are applied while the lower edge is supported rigidly. Both these displacements change in time cyclically, cf. Fig. 15).

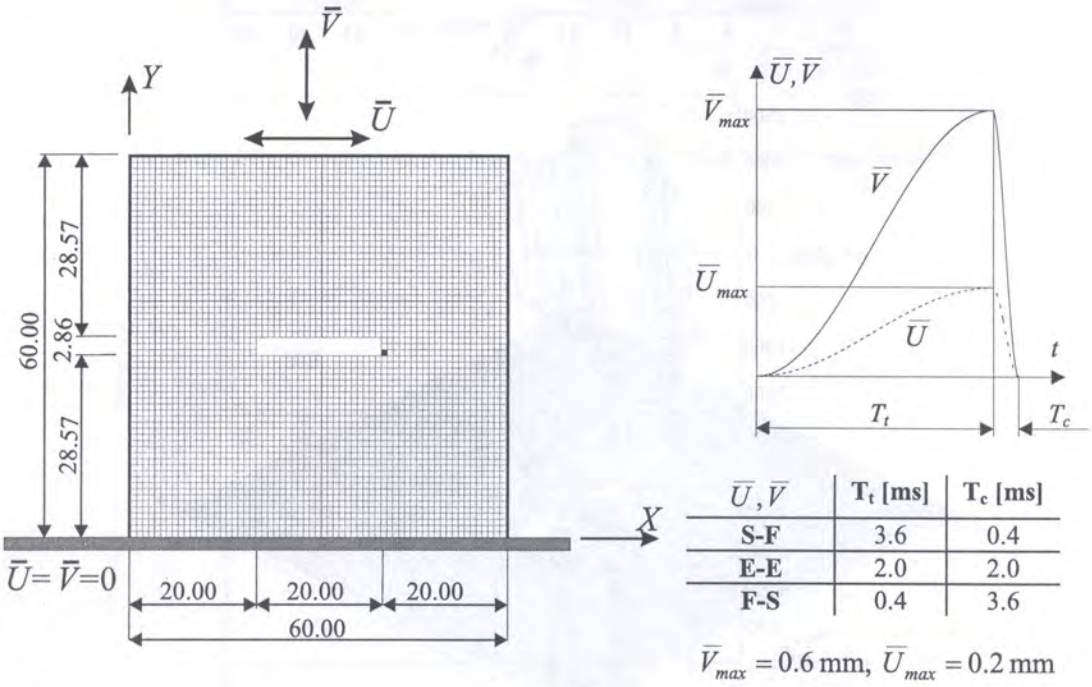

$\overline{U},\overline{V}$	T_t [ms]	T_c [ms]
S-F	3.6	0.4
E-E	2.0	2.0
F-S	0.4	3.6

$\overline{V}_{max} = 0.6$ mm, $\overline{U}_{max} = 0.2$ mm

Fig. 15. Geometry, kinematic constraints and finite difference discretization (4096 nodes) of the thin steel plate with small rectangular hole located in the center (all dimensions are in milimeters)

It has been assumed that both displacements have the same character of change in time.

We consider the cyclic displacement constraints in the form of the three different loading characteristics (adiabatic and isothermal) in time, namely slow–fast, equal–equal and fast–slow, cf. Fig. 15. All three types of constraints are represented by positive cycles, pulsating from zero and having same amplitudes: $\overline{V}_{max} = 0.6$ mm, $\overline{U}_{max} = 0.2$ mm, and the same period. They have different time for tensile deformation T_t and compress deformation T_c in a cycle as it has been shown in Fig. 15. The tensile and compress constraints are described by the sine functions as follows:

$$\left.\begin{matrix} V_t \\ U_t \end{matrix}\right\} = \frac{1}{2}\left[\begin{matrix} \overline{V}_{max} \\ \overline{U}_{max} \end{matrix} \sin\pi\left(\frac{t}{T_t} - \frac{1}{2}\right) + \begin{matrix} \overline{V}_{max} \\ \overline{U}_{max} \end{matrix}\right], \qquad t \in (0, T_t), \tag{111}$$

$$\left.\begin{matrix} V_c \\ U_c \end{matrix}\right\} = \frac{1}{2}\left[\begin{matrix} \overline{V}_{max} \\ \overline{U}_{max} \end{matrix} \sin\pi\left(\frac{t}{T_c} + \frac{1}{2}\right) + \begin{matrix} \overline{V}_{max} \\ \overline{U}_{max} \end{matrix}\right], \qquad t \in (0, T_c). \tag{112}$$

The material of a plate is AISI 4340 steel. It has been assumed very dense mesh, namely $N \times M = 64 \times 64 = 4096$ nodes.

The influence of the wave shape and temperature on the $\sigma^{YY} - e_{YY}$ relation has been shown in Fig. 16 (all results concern the node near the tip of the rectangular hole, see the black quadrangle

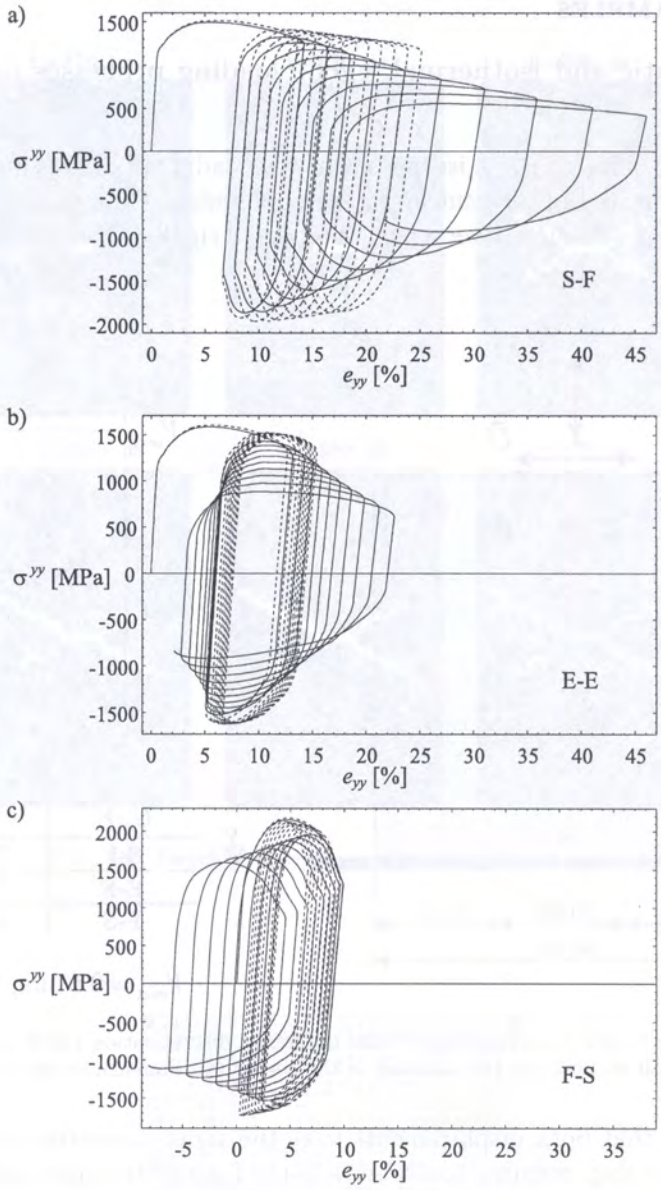

Fig. 16. Influence of the wave shape and temperature on the $\sigma^{YY} - \mathbf{e}_{YY}$ relation, solid line – adiabatic process, dashed line – isothermal process, (a) slow–fast, (b) equal–equal, (c) fast–slow

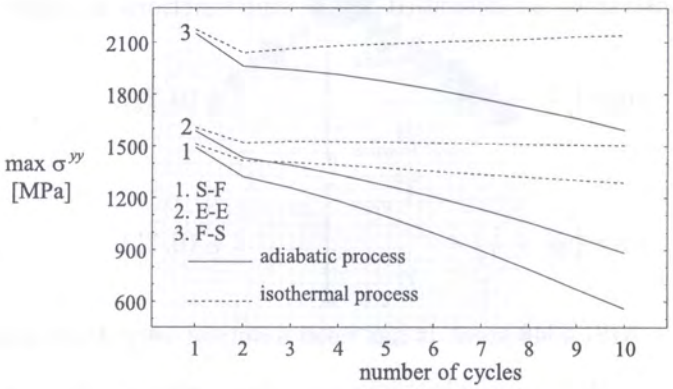

Fig. 17. Maximum stress σ^{YY} per cycle as a function of number of cycles

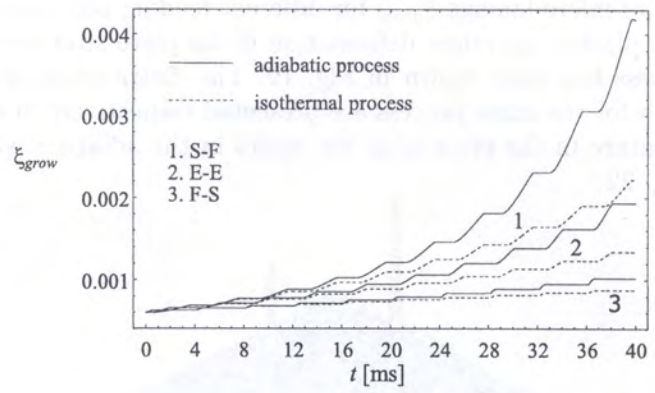

Fig. 18. Evolution of the damage ξ_{grow} for different loading processes

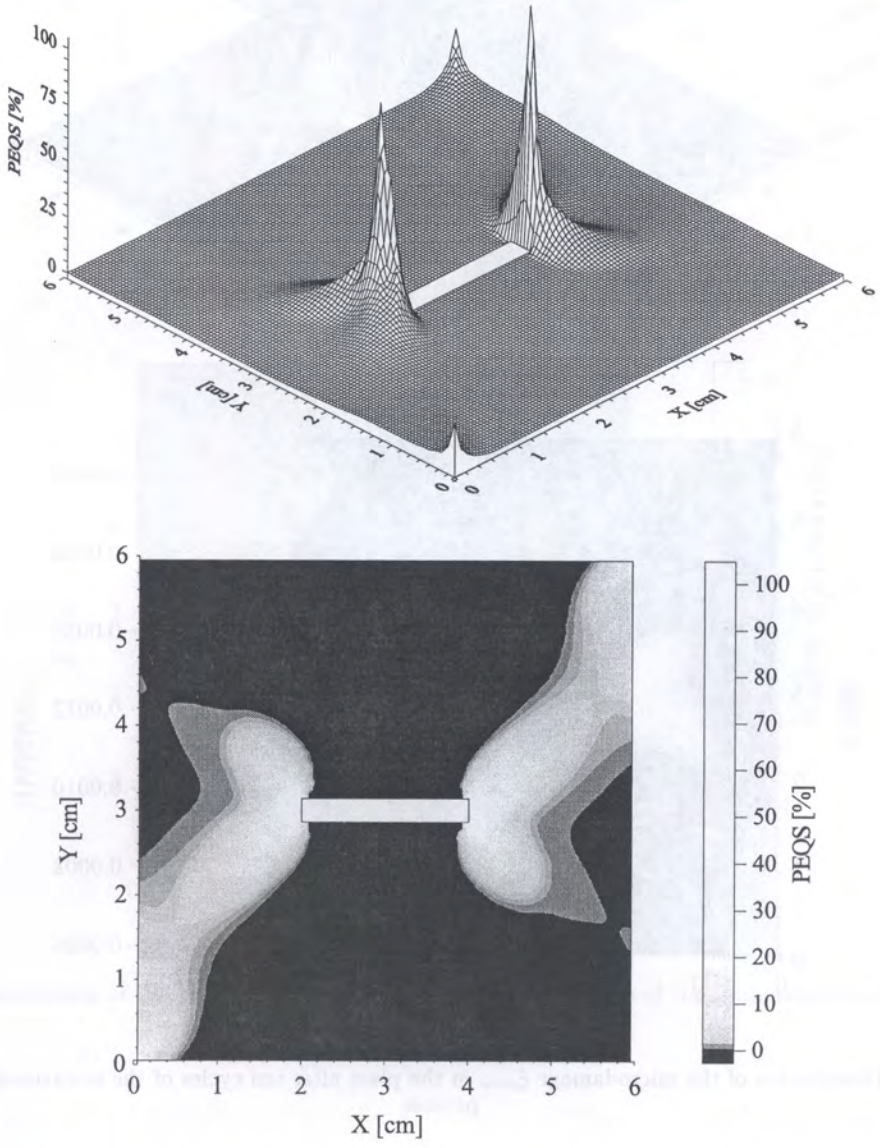

Fig. 19. Distribution of the plastic equivalent strain in the plate after ten cycles of the isothermal slow–fast process

in Fig. 15). The maximum stress σ^{YY} per cycle as a function of number of cycles is plotted in Fig. 17. The evolution of microdamage ξ_{grow} for different loading processes is presented in Fig. 18. The distribution of the plastic equivalent deformation in the plate after ten cycles in the isothermal slow–fast loading process has been shown in Fig. 19. The distribution of the microdamage ξ_{grow} and the plastic rotation for the same process are presented respectively in Fig. 20 and Fig. 21. The distribution of temperature in the plate after ten cycles in the adiabatic slow–fast loading process has been shown in Fig. 22.

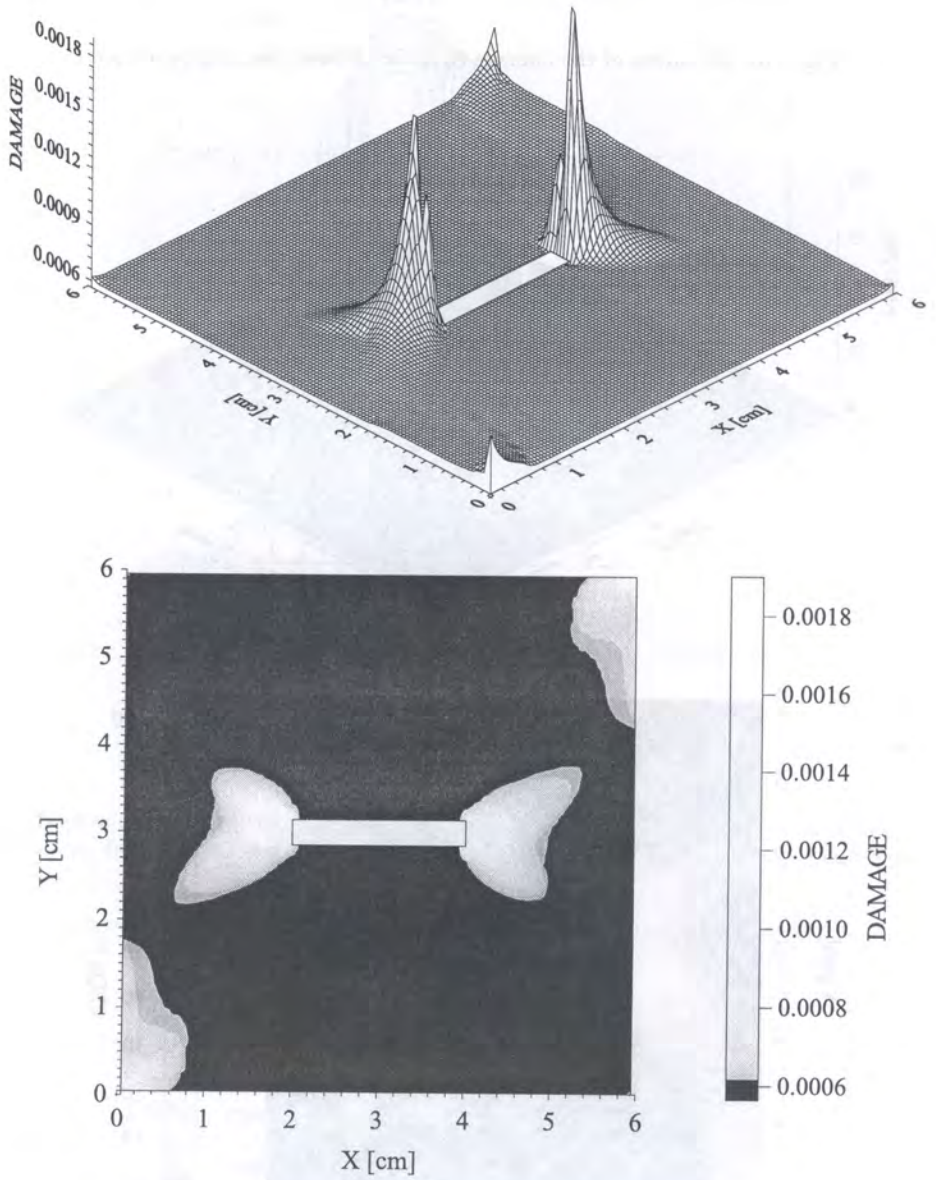

Fig. 20. Distribution of the microdamage ξ_{grow} in the plate after ten cycles of the isothermal slow–fast process

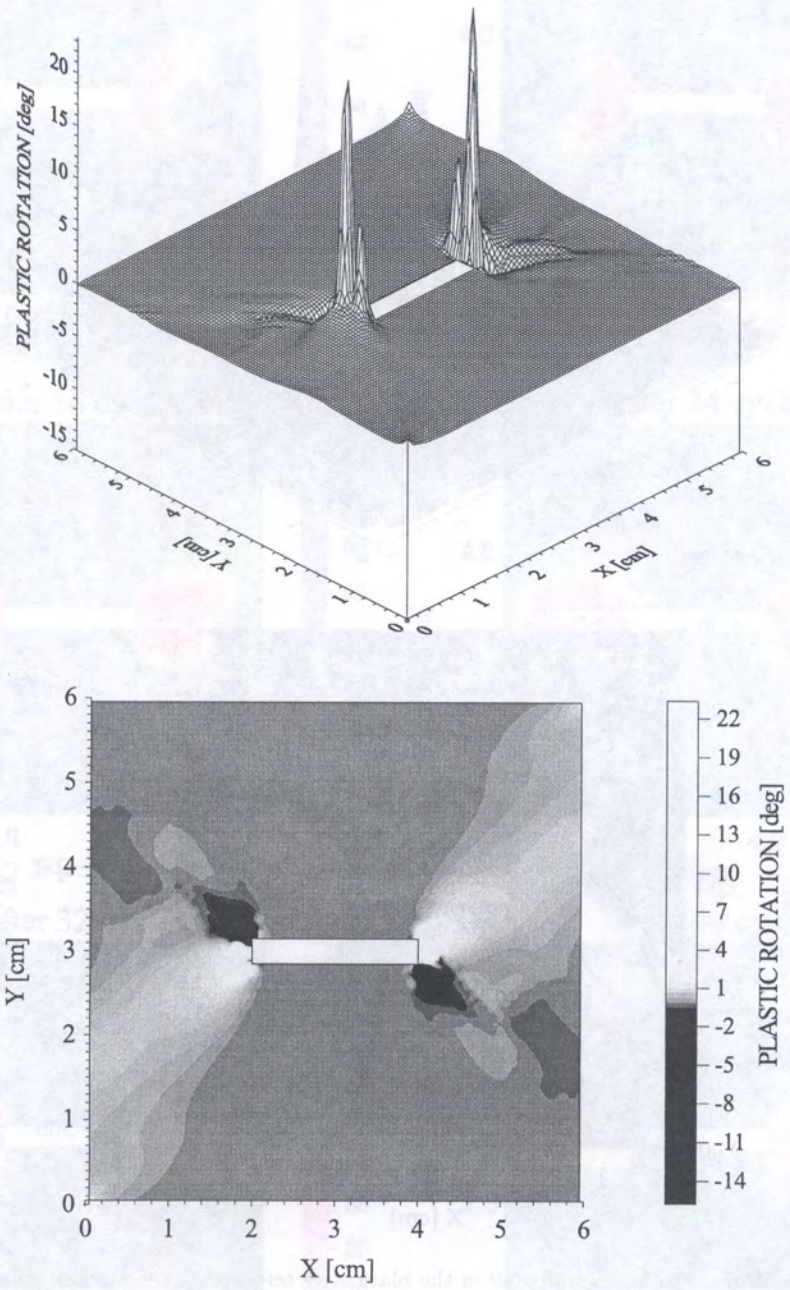

Fig. 21. Distribution of the plastic rotation in the plate after ten cycles of the isothermal slow–fast process

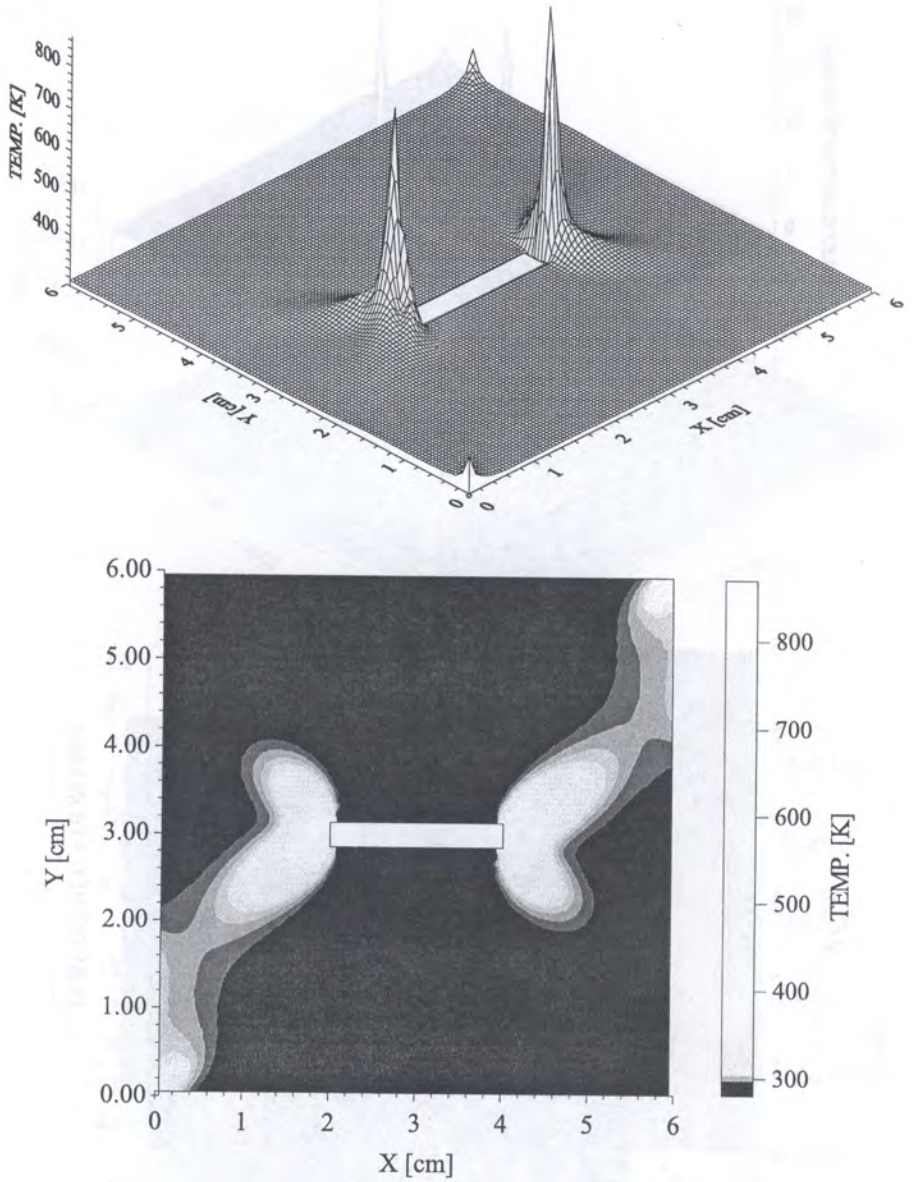

Fig. 22. Distribution of the termperature ϑ in the plate after ten cycles of the adiabatic slow–fast process

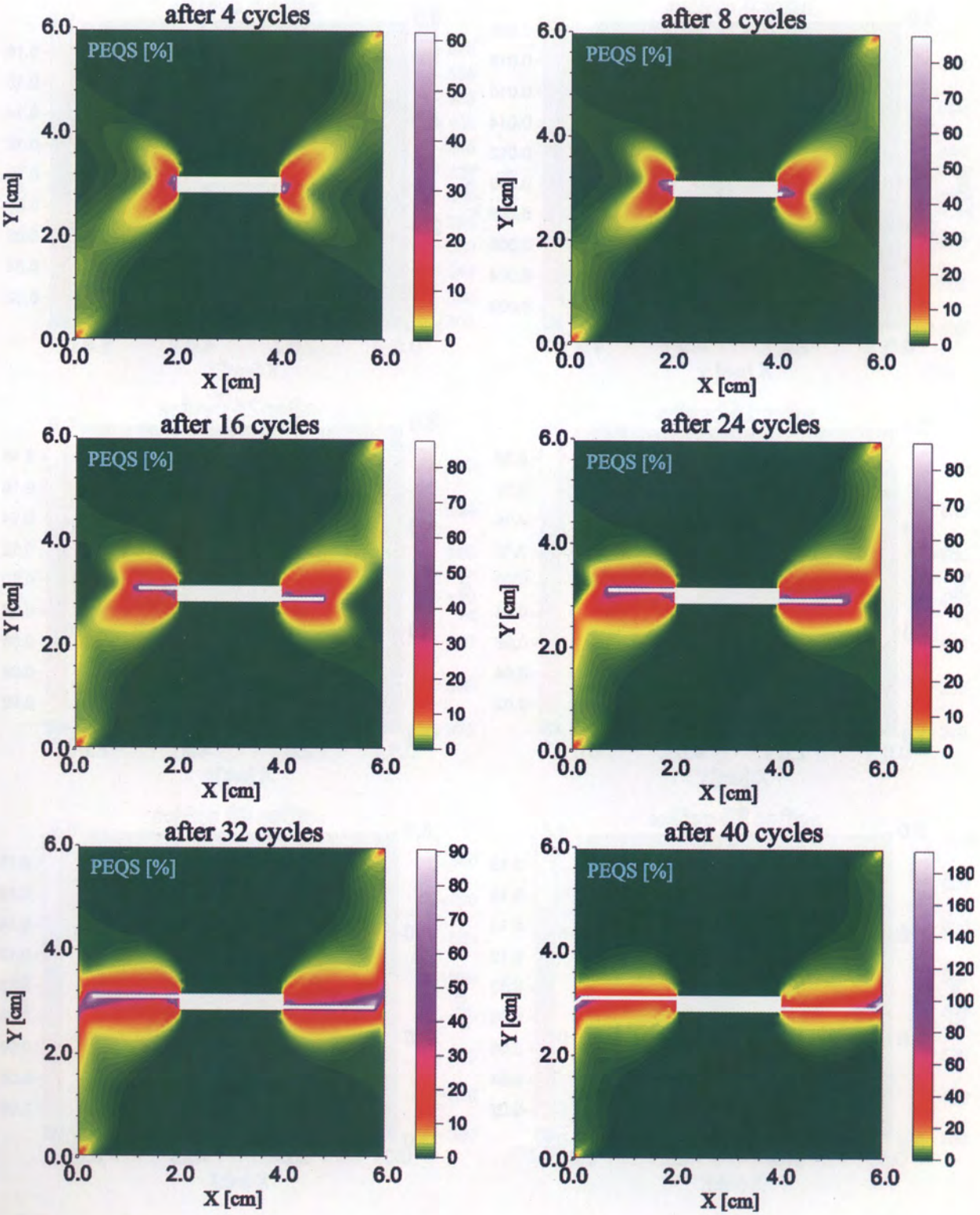

Fig. 23. Evolution of the equivalent plastic deformation in the vicinity of the developed fatigue damage as function of number of cycles

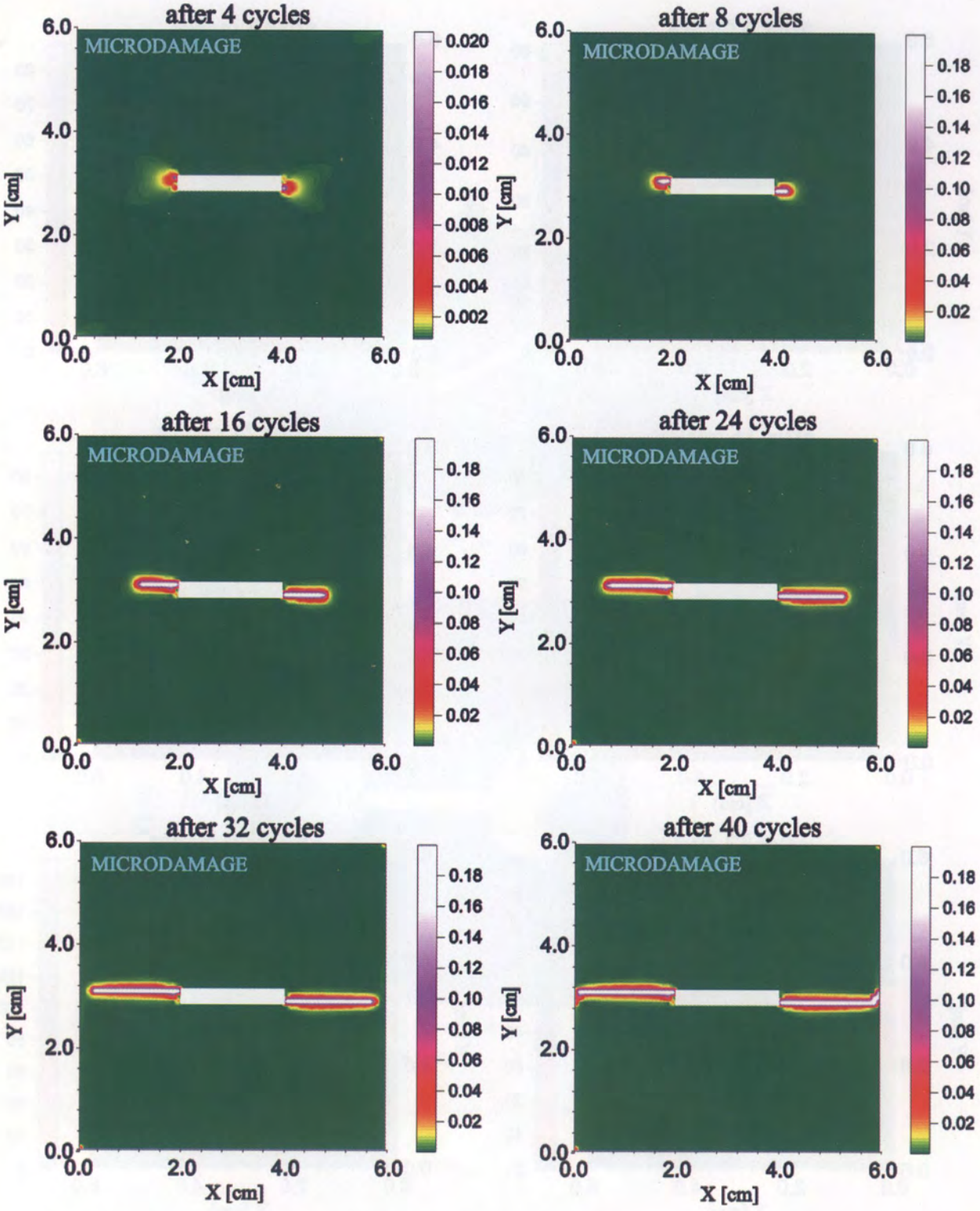

Fig. 24. Evolution of microdamage in the vicinity of the developed fatigue damage as function of number of cycles

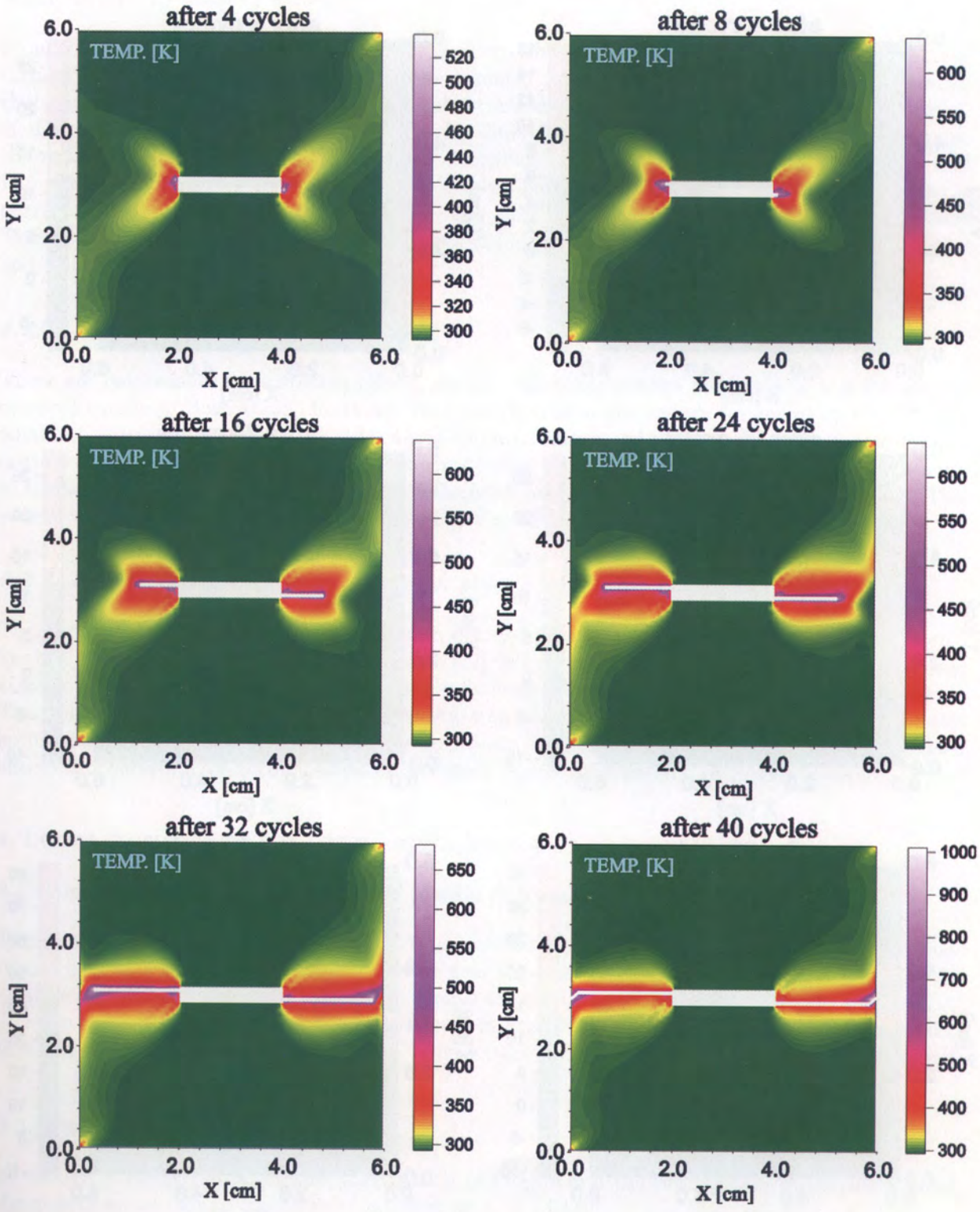

Fig. 25. Distribution of temperature ϑ in the vicinity of the developed fatigue damage as function of number of cycles

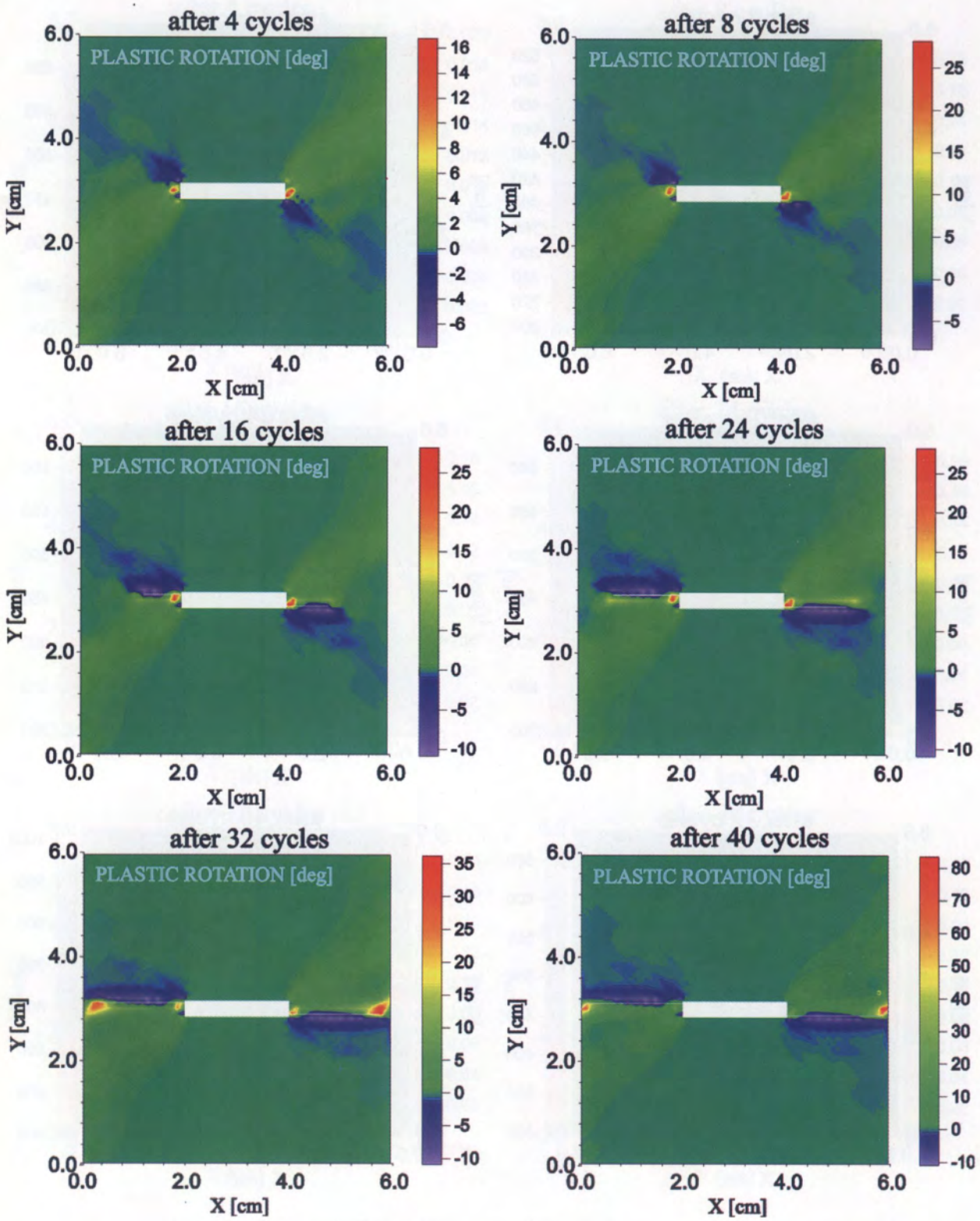

Fig. 26. Distribution of the plastic rotation in the vicinity of the developed fatigue damage as function of number of cycles

8.2. Analysis of the influence of various effects

8.2.1. Shape of loading waves

From the results presented in Figs. 16–18 it is clearly shown that the accumulation of microdamage distinctly depends on the wave shape of the assumed loading cycle. The condition can be drown that cycles with longer time of applied tensile stress lead sooner to the softening of the material, cf. Fig. 18. Different strain rate in a cycle for different kind of adiabatic process influences the character of changes of the consider stress. Difference in amplitude of tensile stress for S–F and F–S loadings are implied by viscosity of a material. For all cases the effect of plastic hardening is characteristic. The saturation of hardening is first observed for S–F loading process (after 5 cycles). These conclusions are in good agreement with the experimental observations presented by Sidey and Coffin [64].

8.2.2. Softening effects

There are two reasons for softening effects, namely the microdamage mechanisms and thermomechanical coupling. Both these effects are very well visible in the results presented in Fig. 17. For adiabatic process the softening effect is caused by both reasons and is very high, while for isothermal process the softening is generated only by microdamage mechanisms and is smaller. It is noteworthy to stress that the microdamage process is influenced very much by thermomechanical effects. This is very well visible from the results presented in Fig. 18.

8.2.3. Plastic strain induced anisotropy, plastic spin and covariant terms

The particular discussion of the plastic strain induced anisotropy, plastic spin and covariant terms has been presented by Dornowski and Perzyna [22]. It has been found that the plastic strain induced anisotropy described by kinematic hardering influences very much through the plastic spin effects. There is observed the accumulation of the plastic spin effects and very pronounced differences for this accumulation for isothermal and adiabatic processes. Similarly, the accumulation of the covariant effects is observed. This accumulation is also much higher for adiabatic processes.

9. Localization and fracture phenomena

9.1. Discussion of the localization of plastic deformation

The results presented in Fig. 19 have clearly shown the localization phenomena of plastic deformation in small two asymmetric regions located near the tips of the rectangular hole. Of course, the localization is very much diffused, what is typical for an elastic-viscoplastic model of a material.

From the examination of the results presented in Figs. 20, 21 and 22 we can draw the conclusion that also the distributions of microdamage, temperature and plastic rotation are very much localized.

9.2. Discussion of fatigue damage

In numerical computation for the investigation of fatigue and the propagation of the macrocrack the growth micro-damage constant is assumed as $c_1 = 1.047$.

The evolution of the equivalent plastic deformation in the vicinity of the developed fatigue damage as function of number of cycles is presented in Fig. 23. In Figs. 24, 25 and 26 the evolution of microdamage, temperature and plastic rotation in the vicinity of the developed fatigue damage as function of number of cycles are showed, respectively. The length of macroscopic fatigue damage crack versus number of cycles for slow–fast loading process has been presented in Fig. 27.

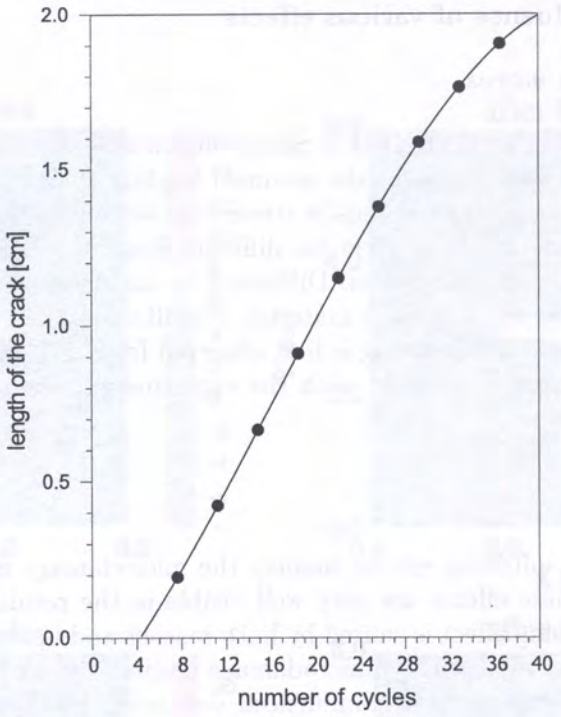

Fig. 27. The length of macroscopic fatigue damage crack versus number of cycles

These results have clearly shown the fatigue damage phenomena in a thin steel plate with small rectangular hole located in the centre subjected to plastic flow process under dynamic loadings.

The results obtained for a dynamic adiabatic cyclic loading process for a thin plate have approved that the developed thermo-elasto-viscoplastic theory represents very useful model for the description of the fatugue damage.

10. Final comments

We hope that a new constitutive model proposed is sufficiently simple in its nature that it can be applicable to the numerical solution of initial-boundary value problems under cyclic loadings.

The crucial idea in this theory is the very efficient interpretation of a finite set of the internal state variables as the equivalent plastic deformation, volume fraction porosity and the residual stress (the back stress). To describe suitably the time and temperature dependent effects observed experimentally and the accumulation of the plastic deformation and damage during dynamic cyclic loading process the kinetics of microdamage and the kinematic hardening law have been modified. To show how the modification of the evolution equation for the porosity parameter ξ helps to describe the accumulation of damage during dynamic cyclic loading process the evolution of the microdamage ξ_{grow} in a node near the tip of the hole (black quadrangle) for different forms of the stress intensity invariant for adiabatic process and various wave shape loadings is presented in Fig. 28.

The performed numerical simulations of the dynamic, cyclic loading process have proven the usefulness of the thermo-elasto-viscoplastic theory. The viscoplastic regularization procedure assures the stable integration algorithm by using the finite difference method. Convergence, consistency, and stability of the discretised problem are discussed. The Lax–Richtmyer equivalence theorem is formulated and conditions under which this theorem is valid are examined. The accumulation of damage and equivalent plastic deformation on each considered cycle has been obtained. It has been numerically found that accumulation of microdamage distinctly depends on the wave shape of the assumed loading cycle.

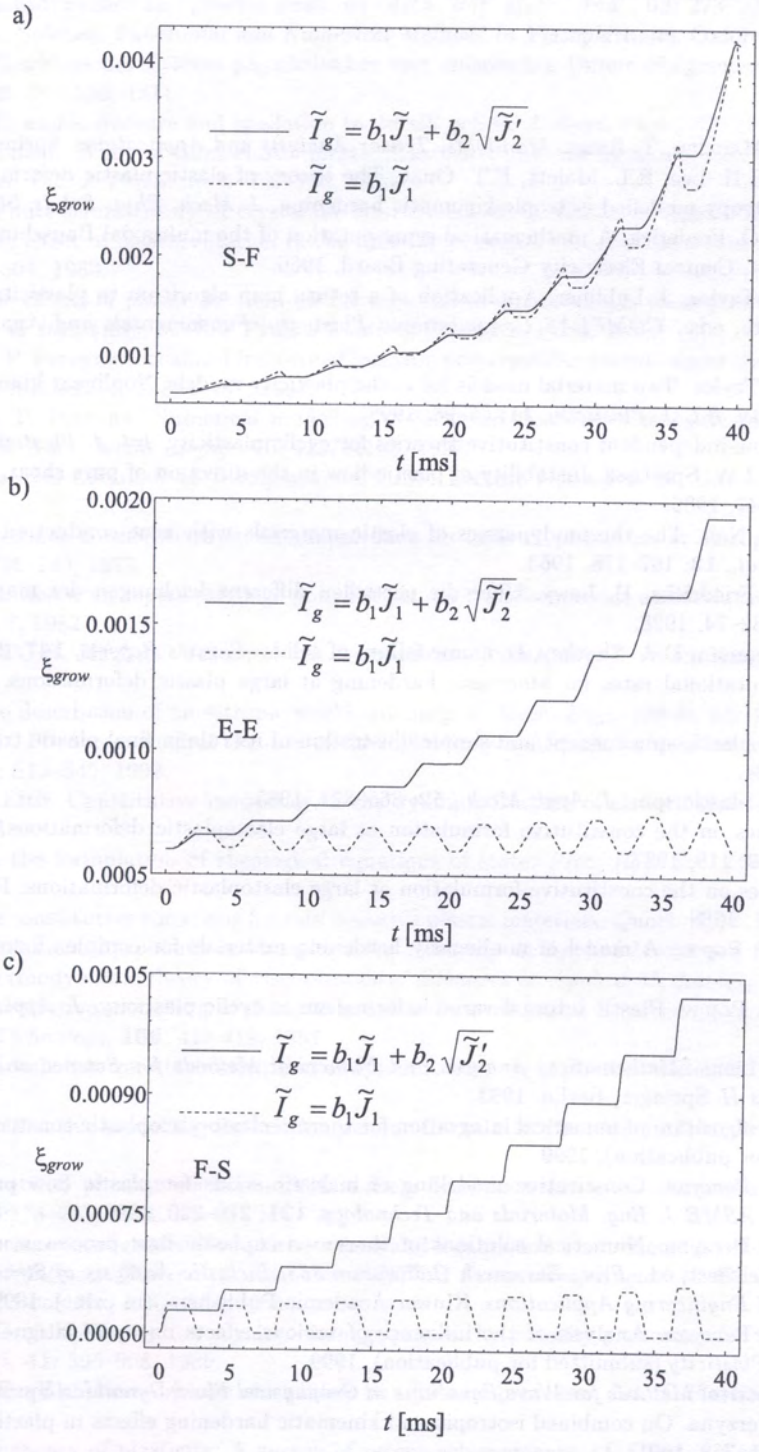

Fig. 28. Evolution of the damage ξ_{grow} for different forms of the stress intensity invariant (adiabatic process), (a) slow–fast, (b) equal–equal, (c) fast–slow

ACKNOWLEDGMENT

The paper has been partly prepared within the research programme sponsored by the Committee of Scientific Research under Grant 7 T07 A006 16.

REFERENCES

[1] R. Abraham, J.E. Marsden, T. Ratiu. *Manifolds, Tensor Analysis and Applications.* Springer, Berlin, 1988.

[2] A. Agah-Tehrani, E.H. Lee, R.L. Malett, E.T. Onat. The theory of elastic-plastic deformation at finite strain with induced anisotropy modelled isotropic-kinematic hardening. *J. Mech. Phys. Solids*, **35**: 43–60, 1987.

[3] P.J. Armstrong, C.O. Frederick. A mathematical representation of the multiaxial Bauschinger effect. In: *CEGB Report RD/B/N731*, Central Electricity Generating Board, 1966.

[4] F. Auricchio, R.L. Taylor, J. Lubliner. Application of a return map algorithm to plasticity models. In: D.R.J. Owen and E. Oñate, eds., *COMPLAS Computational Plasticity: Fundamentals and Applications*, 2229–2248. Barcelona, 1992.

[5] F. Auricchio, R.L. Taylor. Two material models for cyclic plasticity models: Nonlinear kinematic hardening and generalized plasticity. *Int. J. Plasticity*, **11**: 65–98, 1995.

[6] J.L. Chaboche. Time-independent constitutive theories for cyclic plasticity. *Int. J. Plasticity*, **2**: 149–188.

[7] A.K. Chakrabarti, J.W. Spretnak. Instability of plastic flow in the direction of pure shear. *Metallurgical Transactions*, **6A**: 733–747, 1986.

[8] B.D. Coleman, W. Noll. The thermodynamics of elastic materials with heat conduction and viscosity. *Arch. Rational Mech. Anal.*, **13**: 167–178, 1963.

[9] R. Courant, K.O. Friedrichs, H. Lewy. Uber die partiellen differenzgleichungen der mathematischen physik. *Math. Ann.*, **100**: 32–74, 1928.

[10] D.R. Curran, L. Seaman, D.A. Shockey. Dynamic failure of solids. *Physics Reports*, **147**: 253–388, 1987.

[11] Y.F. Dafalias. Corotational rates for kinematic hardening at large plastic deformations. *J. Appl. Mech.*, **50**: 561–565, 1983.

[12] Y.F. Dafalias. The plastic spin concept and simple illustration of its rule in final plastic transformations. *Mech. Mater.*, **3**: 223, 1984.

[13] Y.F. Dafalias. The plastic spin. *J. Appl. Mech.*, **52**: 865–871, 1985.

[14] Y.F. Dafalias. Issues on the constitutive formulation at large elastoplastic deformations, Part 1: Kinematics. *Acta Mechanica*, **69**: 119, 1987.

[15] Y.F. Dafalias. Issues on the constitutive formulation at large elastoplastic deformations, Part 2: Kinetics. *Acta Mechanica*, **73**: 121, 1988.

[16] Y.F. Dafalias, E.P. Popov. A model of nonlinearly hardening materials for complex loading. *Acta Mech.*, **21**: 173–192, 1975.

[17] Y.F. Dafalias, E.P. Popov. Plastic internal variable formalism of cyclic plasticity. *J. Appl. Mech.*, **43**: 645–651, 1976.

[18] R. Dautray, J.-L. Lions. *Mathematical Analysis and Numerical Methods for Science and Technology*, Vol. 6. *Evolution Problems II.* Springer, Berlin, 1993.

[19] W. Dornowski. An algorithm of numerical integration for thermo-elasto-viscoplastic constitutive equations. *Biul. WAT* (submitted for publication), 1999.

[20] W. Dornowski, P. Perzyna. Constitutive modelling of inelastic solids for plastic flow processes under cyclic dynamic loadings. *ASME J. Eng. Materials and Technology*, **121**: 210–220, 1999.

[21] W. Dornowski, P. Perzyna. Numerical solutions of thermo-viscoplastic flow processes under cyclic dynamic loadings. In: D. Weichert, ed., *Proc. Euromech Colloquium 383, Inelastic Analysis of Structures under Variable Loads: Theory and Engineering Applications.* Kluwer Academic Publishers, (in print), 1999.

[22] W. Dornowski, P. Perzyna. Analysis of the influence of various effects on cycle fatigue damage in dynamic processes. *Int. J. Plasticity* (submitted for publication), 1999.

[23] D.R. Durran. *Numerical Methods for Wave Equations in Geophysical Fluid Dynamics.* Springer, New York, 1999.

[24] M.K. Duszek, P. Perzyna. On combined isotropic and kinematic hardening effects in plastic flow processes. *Int. J. Plasticity*, **7**: 351–363, 1991.

[25] M.K. Duszek, P. Perzyna. The localization of plastic deformation in thermoplastic solids. *Int. J. Solids Structures*, **27**: 1419–1443, 1991.

[26] M.K. Duszek-Perzyna, P. Perzyna. Analysis of the influence of different effects on criteria for adiabatic shear band localization in inelastic solids. In: R.C. Batra, H.M. Zbib, eds., *Material Instabilities: Theory and Applications. ASME Congress, Chicago, 9–11 November 1994*, AMD-Vol. 183/MD-Vol.50, 59–85. ASME, New York, 1994.

[27] M.K. Duszek-Perzyna, P. Perzyna. Analysis of anisotropy and plastic spin on localization phenomena. *Arch. Appl. Mechanics*, **68**: 352–374, 1998.

[28] B. Gustafsson, H.O. Kreiss, J. Oliger. *Time Dependent Problems and Difference Methods.* John Wiley, New York, 1995.
[29] B. Halphen. Sur le champ des vitesses en thermoplasticité finie. *Int. J. Solids Structures*, **11**: 947, 1975.
[30] T.J.R. Hughes, T. Kato, J.E. Marsden. Well-posed quasilinear second order hyperbolic system with application to nonlinear elastodynamics and general relativity. *Arch. Rat. Mech. Anal.*, **63**: 273–294, 1977.
[31] I.R. Ionescu, M. Sofonea. *Functional and Numerical Methods in Viscoplasticity.* Oxford, 1993.
[32] G. Jaumann. Geschlossenes System physikalischer und chemischer Differentialgesetze. *Sitzgsber. Akad. Wiss. Wien (IIa)*, **120**: 385–530, 1911.
[33] J.N. Johnson. Dynamic fracture and spallation in ductile solids. *J. Appl. Phys.*, **52**: 2812–2825, 1981.
[34] A.S. Khan, P. Cheng. Study of three elastic-plastic constitutive models by non-proportional finite deformations of OFHC copper. *Int. J. Plasticity*, **6**: 737–759, 1996.
[35] J. Kratochvil. Finite-strain theory of crystalline elastic-inelastic materials. *J. Appl. Phys.*, **42**: 1104, 1971.
[36] B. Loret. On the effect of plastic rotation in the finite deformation of anisotropic elastoplastic materials. *Mech. Mater.*, **2**: 287–304, 1983.
[37] B. Loret. On the effects of plastic rotation on the localization of anisotropic elastoplastic solids. In: J. Salencon et al., eds. *Plastic Instability*, 89–100. Presses Ponts et Chausees, Paris, 1985.
[38] T. Łodygowski, P. Perzyna. Localized fracture of inelastic polycrystalline solids under dynamic loading processes. *Int. J. Damage Mechanics*, **6**: 364–407, 1997.
[39] T. Łodygowski, P. Perzyna. Numerical modelling of localized fracture of inelastic solids in dynamic loading processes. *Int. J. Num. Meth. Engng.*, **40**: 4137–4158, 1997.
[40] J. Mandel. *Plasticité Classique et Viscoplasticite.* CISM Lecture Notes No. 97, Udine, Springer-Verlag, Wien, 1971.
[41] J. Mandel. Equations constitutives et directeurs dans les milieux plastiques et viscoplastiques. *Int. J. Solids Structures*, **9**: 725–740, 1973.
[42] J. Mandel. Définition d'un repère privilégé pour l'etude des transformations anélastiques du polycrystal. *J. Méc. Théo. Appl.*, **1**: 7, 1982.
[43] J.E. Marsden, T.J.R. Hughes. *Mathematical Foundations of Elasticity.* Prentice-Hall, Englewood Cliffs, New York, 1983.
[44] Z. Mróz. On the description of anisotropic workhardening. *J. Mech. Phys. Solids*, **15**: 163–175, 1967.
[45] S. Nemat-Nasser. Phenomenological theories of elastoplasticity and strain localization at high strain rates. *Appl. Mech. Rev.*, **45**: S19–S45, 1992.
[46] J.A. Nemes, J. Eftis. Constitutive modelling on the dynamic fracture of smooth tensile bars. *Int. J. Plasticity*, **9**:243–270, 1993.
[47] J. Oldroyd. On the formulation of rheological equations of state. *Proc. Roy. Soc. (London)*, **A 200**: 523–541, 1950.
[48] P. Perzyna. The constitutive equations for rate sensitive plastic materials. *Quart. Appl. Math.*, **20**:321–332, 1963.
[49] P. Perzyna. Fundamental problems in viscoplasticity. *Advances in Applied Mechanics*, **9**: 343–377, 1966.
[50] P. Perzyna. Thermodynamic theory of viscoplasticity. *Advances in Applied Mechanics*, **11**: 313–354, 1971.
[51] P. Perzyna. Constitutive modelling of dissipative solids for postcritical behaviour and fracture. *ASME J. Eng. Materials and Technology*, **106**: 410-419, 1984.
[52] P. Perzyna. Internal state variable description of dynamic fracture of ductile solids. *Int. J. Solids Structures*, **22**: 797-818, 1986.
[53] P. Perzyna. Constitutive modelling for brittle dynamic fracture in dissipative solids. *Arch. Mechanics*, **38**: 725–738, 1986.
[54] P. Perzyna. Instability phenomena and adiabatic shear band localization in thermoplastic flow processes. *Acta Mechanica*, **106**:173–205, 1994.
[55] P. Perzyna. Interactions of elastic-viscoplastic waves and localization phenomena in solids. In: L.J. Wegner, F.R. Norwood, eds., *Nonlinear Waves in Solids, Proc. IUTAM Symposium, August 15–20, 1993, Victoria, Canada*, 114–121. ASME Book No. AMR 137, 1995.
[56] P. Perzyna, A. Drabik. Description of micro-damage process by porosity parameter for nonlinear viscoplasticity. *Arch. Mechanics*, **41**: 895–908, 1989.
[57] P. Perzyna, A. Drabik. Micro-damage mechanism in adiabatic processes. *Int. J. Plasticity* (submitted for publication), 1999.
[58] W. Prager. The theory of plasticity: A survey of recent achievements. (J. Clayton Lecture), *Proc. Inst. Mech. Eng.*, **169**: 41–57, 1955.
[59] R.D. Richtmyer. *Principles of Advance Mathematical Physics.* Vol. I, Springer, New York, 1978.
[60] R.D. Richtmyer, K.W. Morton. *Difference Methods for Initial-Value Problems.* John Wiley, New York, 1967.
[61] M. Ristinmaa. Cyclic plasticity model using one yield surface only. *Int. J. Plasticity*, **11**: 163–181, 1995.
[62] S. Shima, M. Oyane. Plasticity for porous solids. *Int. J. Mech. Sci.*, **18**: 285–291, 1976.
[63] D.A. Shockey, L. Seaman, D.R. Curran. The microstatistical fracture mechanics approach to dynamic fracture problem. *Int. J. Fracture*, **27**: 145–157, 1985.

[64] D. Sidey, L.F. Coffin. Low-cycle fatigue damage mechamisms at high temperature. In: J.T. Fong, ed., *Fatigue Mechanism*, Proc. ASTM STP 675 Symposium, Kansas City, Mo., May 1978, 528–568. Baltimore, 1979.

[65] G. Strang, G.J. Fix. *An Analysis of the Finite Element Method.* Prentice-Hall, Englewood Cliffs, 1973.

[66] C. Truesdell, W. Noll. *The nonlinear field theories*, 1–579. Handbuch der Physik, Band III/3. Springer, Berlin, 1965.

[67] E. Van der Giessen. Continuum models of large deformation plasticity, Part I: Large deformation plasticity and the concept of a natural reference state. *Eur. J. Mech., A/Solids*, **8**: 15, 1989.

[68] E. Van der Giessen. Continuum models of large deformation plasticity, Part II: A kinematic hardening model and the concept of a plastically induced orientational structure. *Eur. J. Mech., A/Solids*, **8**: 89, 1989.

[69] E. Van der Giessen. Micromechanical and thermodynamic aspects of the plastic spin. *Int. J. Plasticity*, **7**: 365–386, 1991.

[70] J.-D. Wang, N. Ohno. Two equivalent forms of nonlinear kinematic hardening: application to nonisothermal plasticity. *Int. J. Plasticity*, **7**: 637–650, 1991.

[71] S. Zaremba. Sur une forme perfectionnée de la théorie de la relaxation. *Bull. Int. Acad. Sci. Cracovie*, 594–614, 1903.

[72] S. Zaremba. Le principe des mouvements relatifs et les équations de la mécanique physique. *Bull. Int. Acad. Sci. Cracovie*, 614–621, 1903.

[73] H. Ziegler. A modification of Prager's hardening rule. *Quart. Appl. Math.*, **17**: 55–65, 1959.